PRIMARY AND SECONDARY DENDRITE ARM SPACING IN UNIDIRECTIONALLY SOLIDIFIED Al-2%Cu

by

S.Hüge Gürer

B.S. in M.E., Boğaziçi University, 1980

Submitted to the Institute for Graduate Studies in Science and Engineering in partial fulfillment of the requirements for the degree of

Master of Science

in

Mechanical Engineering

Boğaziçi University

1983

A C K N O W L E D G E M E N T S

The author wishes to express her gratitude to Doç.Dr.S. Ergin Kısakürek for his valuable guiding help during the course of this study.

Thanks are also due to the members of his committee for their comments, suggestions and assistance.

Special thanks are due to Doç.Dr.Sabri Altıntaş and Dr. Vahan Kalenderoğlu whose invaluable assistance and suggestions were always there at the crucial problems of this study.

Sincere appreciation goes to Timuçin Gürer, Serdar Görgüç, Tuğrul Misoğlu, Semih Sökmen and Tuğrul Tekbulut for their help with the technical details of this study and heartening.

The author is also indepted to the technical staff of the faculty for their help in the construction and photographing.

A B S T R A C T

In this study unidirectionally controlled solidification of Al-2%Cu alloy and the resulting dendritic morphology is investigated. First general information is given on solidification, then dendritic growth is studied thoroughly.

In experimental work, Al-2%Cu has been solidified under controlled laboratory conditions. For this purpose, a unidirectional growth furnace and a drive system has been designed and constructed. With the aid of this system, desired temperature gradient(G_L) and growth rate(R) has been obtained during the experiments. Using a G_L range between 10-40^{o}C/cm and an R range between 1-50x10^{-3}cm/sec, dendritic morphology has been obtained. The liquid-solid interface has been frozen during growth by quenching. The resulting growth surfaces have been cut perpendicular to and parallel to growth direction, photographed and measured. The measured primary and secondary arm spacings have been correlated to the changes in growth conditions, i.e. growth rate and temperature gradient.

ÖZET

Bu çalışmada Al-2%Cu alaşımının kontrollü yönlendirilmiş katılaşması ve oluşan dendrit morfolojisi incelenmiştir. Önce katılaşma üzerine genel bir bilgi verilmiş olup daha sonra dendritik büyüme etraflıca incelenmiştir.

Deneysel çalışmalarda Al-2%Cu alaşımının kontrollü laboratuvar şartlarında katılaşması gerçekleştirilmiştir. Bu amaçla bir yönlendirilmiş katılaştırma fırını ve hareket sistemi dizayn edilip kurulmuş ve deneylerde istenilen sıcaklık gradyanı(G_L) ve katılaşma hızının(R) parametre olarak elde edilmesi sağlanmıştır. 10-40^{o}C/cm arasında sıcaklık gradyanı ve 1-50x10^{-3}cm/sn arasında hız kullanmak suretiyle kontrollü şartlar altında katılaşma yoluyla dendiritik yapı elde edilmiştir. Katılaşma esnasında su verilerek katı-sıvı bölgesinin sabit kalması sağlanmıştır. Daha sonra büyüme yönüne dik ve paralel kesitlerin mikroyapı fotoğrafları çekilerek üzerinde incelemeler yapmak suretiyle dendrit birinci ve ikinci kolları arasındaki açıklıklar bulunmuştur. Ölçülen açıklıklarla büyüme şartları(G_L ve R) arasında korelasyona varılmıştır.

TABLE OF CONTENTS

LIST OF TABLES

LIST OF FIGURES

LIST OF SYMBOLS

a	Temperature gradient exponent
b	Growth rate exponent
C	Composition in atom fraction
C_o	Initial concentration
C_{bulk}	Bulk concentration
C_L^*, C_S^*	Liquid and solid compositions at the interface
C_p	Heat capacity of the liquid phase
$\frac{\partial C}{\partial \bar{n}}$	Concentration gradient normal to the interface
d	Distance behind the dendrite tip
d_o	Capillary length
d_t	Cell size at transition
D_L	Diffusion coefficient of solute in the liquid
f_s, f_l	Weight fraction of solid and liquid
G_L	Temperature gradient in the liquid at the interface
$\triangle G_{het}$	Free energy of formation for heterogenous nuclei
$\triangle G_s$	Total surface energy
$\triangle G_v$	Volume free energy difference between liquid and solid phases
H	Heat of transformation
k_o	Equilibrium partition ratio
k_E	Effective partition ratio
K_L, K_S	Thermal conductivity of liquid and solid

L	Latent heat of solid
m_L	Slope of the liquidus line
n	Spherical harmonics order
Pé	Peclet number
r	Critical radius for nucleation
R	Growth rate
S_S, S_L	Entropy of solid and liquid
$\frac{dS}{dx}$	Gradient of supercooling
t_s	Local solidification time
T_E	Equilibrium temperature at the interface
T_L	Equilibrium liquidus temperature
$\Delta T_K, \Delta T_R, \Delta T_S$	Kinetic, curvature and solute undercoolings
U_L, U_S	Non-thermal energies of liquid and solid phases
V	Velocity of the dendrite tip
V_n	Velocity normal to interface
x'	Distance from the interface into the liquid
α	Thermal diffusivity
δ	Diffusion boundary layer thickness
$\Delta\theta$	Dimensionless supercooling
$\Delta\theta_c$	Term reflecting capillary effect
γ_{SL}, γ_{SC}, γ_{LC}	Surface free energy of substrate-liquid, substrate-crystal, liquid crystal interfaces
Γ	Gibbs-Thomson parameter
λ_1, λ_2	Primary and secondary dendrite arm spacing

λ_s	Critical perturbation wavelength
ν	Kinematic viscosity of the melt
Ω	Constant depending on the curvature of the dendrite tip
ρ	Radius of curvature of the dendrite tip
σ^*	Stability criterion constant
ω	Stirring rate

1. Introduction

Dendritic growth is perhaps the most common form of solidification, especially in metals and other systems that freeze with relatively low entropies of transformation. Dendritic or branched growth in alloys generates microsegregation and other internal defects in castings, ingots and weldments. Dendritic microstructure may introduce the effect of hot cracking, suboptimal thoughness, and reduced corrosion resistance. The dendritic microstructure and its effects may be modified by subsequent heat treatments, but they are seldom fully erased. Therefore, the understanding and control of dendritic growth in solidification process is very important in order to achieve specific material properties in final products.

The size of the dendrites influences the homogenization kinetics and mechanical properties. The fineness of columnar dendrites is usually represented in terms of primary and secondary arm spacings. Various studies have been done on dendrite primary and secondary arm spacings.
Most reliable data is obtained from studies retaining unidirectionally solidified structures grown under controlled conditions, i.e. predetermined temperature gradient and growth rate.

Previous works have shown that dendrite arm spacings decrease with increasing temperature gradient or growth rate, following the relationship:

$$\lambda_1, \lambda_2 \propto (G_L R)^{-a}$$

and a is found to be between 0.25-0.5. However, discrepencies are observed between the results.

In the present work, dendrite morphology of Al-2wt.%Cu alloy will be investigated. The solidification of the alloy is performed unidirectionally under steady state controlled conditions. A furnace and a drive system is designed to be able to control temperature gradient and growth rate seperately. The change in dendrite primary and secondary arms in relation to temperature gradient and growth rate is observed.

2. THEORY OF SOLIDIFICATION

The liquid-solid phase transformation takes place in two steps:

1) Nucleation
2) Growth

2.1 Nucleation

Nucleation may be defined as the formation of a new phase in a distinct region of a matter which is seperated from the surrounding by a definite boundary.

For nucleation atoms of the moltem metal must come together in proper crystalline configuration to be stable against the inherent tendency of the very small crystals to melt. The amount of supercooling needed depends on the chemistry, crystallography, and geometry of the solid particles in the melt or in the solid surface in contact with it. The supercooling necessary for nucleation may vary from a fraction of a degree to a few hundred degrees, depending on the nature of nucleati process.

When a solid forms within its own melt without the aid of foreign materials, it is said to nucleate homogenously. Nucle tion in this way requires a large driving force because of th relatively large contribution of surface energy to the total free energy of very small particles. A classical quantitative homogenous nucleation theory treats this problem by consideri the free energy change of a small region of nucleus with radi "r" upon its transformation from liquid to solid. This energy change has two terms: The volume free energy difference between liquid and solid phases for the formation of a spherical cluster of atoms is ΔG_v:

$$\sum \Delta G_v = \Delta G_v \cdot 4/3 \cdot \pi r^3 \quad \text{..... (1)}$$

And the formation of a new phase is associated with the surface free energy, γ_{SL}. Then total surface energy:

$$\sum \Delta G_s = \gamma_{SL} \cdot 4\pi r^2 \quad \text{..... (2)}$$

$$\therefore \sum \Delta G(r) = \sum \Delta G_v + \sum \Delta G_s \quad \text{.....(3)}$$

$$\Delta G(r) = \Delta G_v \frac{4}{3}\pi r^3 + \gamma_{SL} 4\pi r^2 \quad \text{.....(4)}$$

Here, ΔG_v is negative for any spontaneous reaction but γ_{SL} is always positive. $\Delta G(r)$ is obviously a function of radius. Regarding the plot,(Fig.1)

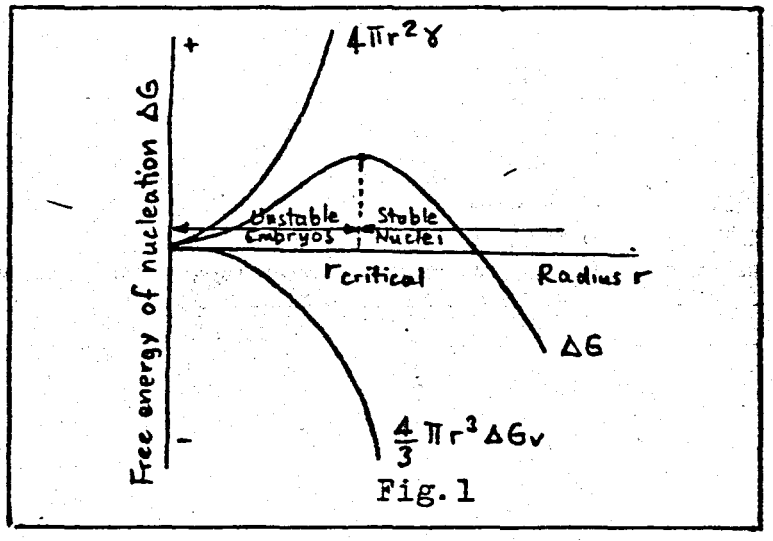

Fig.1

It can be observed that critical radius(r^*) corresponds to the maximum free energy.

$$\left.\frac{d\Delta G(r)}{dr}\right|_{r=r^*} = 0 \quad \text{.....(5)}$$

If $r < r^*$, further growth of the crystallite increases the free energy of the material involved. The atom or molecule groups of solid which are spatially related to each other and have an $r < r^*$ are called "embryos". An embryo becomes a nucleus when it reaches the critical radius size,r^*.

$$\Delta G^*(r) = \sum G(r)\Big|_{r=r^*} \quad \text{.....(6)}$$

We can obtain r^* from Eq.5:

$$\therefore \quad r^* = -\frac{2\gamma_{SL}}{\Delta G_v} \quad \text{.....(7)}$$

and by Eq.6:

$$\Delta G^*(r) = \frac{16}{3}\pi \frac{\gamma_{SL}^3}{\Delta G_v^2} \quad \text{.....(8)}$$

If the liquid is cooled beyond the equilibrium temperature, i.e. supercooled, ΔG_v becomes more negative since:

$$\Delta G_v = U_{solid} - U_{liquid} - T(S_{solid} - S_{liquid}) \quad \text{----------(9)}$$ [1]

where U_L, U_S are "non-thermal energies" of liquid and solid phases respectively per atom

S_S, S_L are the entropy of solid and liquid

At equilibrium temperature, T_E :

$$\Delta G_v = 0 \quad \text{----------(10)}$$

$$\text{or} \quad U_S - U_L = T_E (S_S - S_L) \quad \text{----------(11)}$$

then:

$$S_S - S_L = \frac{U_S - U_L}{T_E} \quad \text{----------(12)}$$

Since $U_S - U_L$ is heat of transformation, i.e. ΔH:

$$\Delta G_v = -\Delta H + \frac{T \Delta H}{T_E} = \frac{\Delta H \Delta T}{T_E} \quad \text{----------(13)}$$

where ΔT is the amount of supercooling. Thus:

$$r^* = -\frac{2 \gamma_{SL} T_E}{\Delta H \Delta T} \quad \text{----------(14)}$$

and

$$\Delta G^*(r) = \frac{16}{3} \pi \frac{\gamma_{SL}^3 T_E^2}{(\Delta H \Delta T)^2} \quad \text{----------(15)}$$

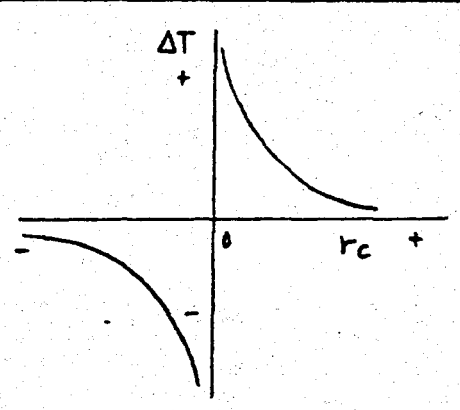

Fig. 2 [1]

Variation of critical radius with temperature

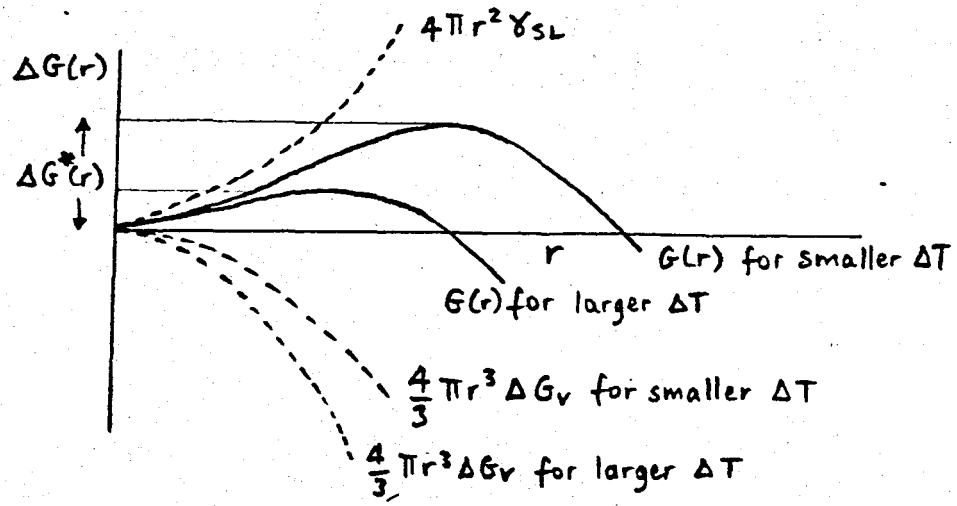

Fig. 3

Effect of supercooling on the critical radius

As the supercooling is increased, the value of ΔG_V becomes more negative(Eq. 13). This reduces both the critical radius and the energy barrier for nucleation.(Fig.3) Thus a greater probability occurs for the necessary number of atoms to attain the appropriate energy for nucleation. As a result, a reaction which can not nucleate at the equilibrium temperature occurs more readily, the greater the undercooling.

Heterogenous Nucleation

It is known that metals and most other liquids rarely undercool by more than a few degrees before beginning to crystallize. The crystallization begins on impurity particles, i.e., nucleating agents or mold walls and by so doing, avoids the very large thermodynamic barrier to homogenous nucleation.

The simplest approach to heterogenous nucleation is to consider a spherical crystalline cluster of atoms at equilibrium on a flat substrate as shown in figure 4.

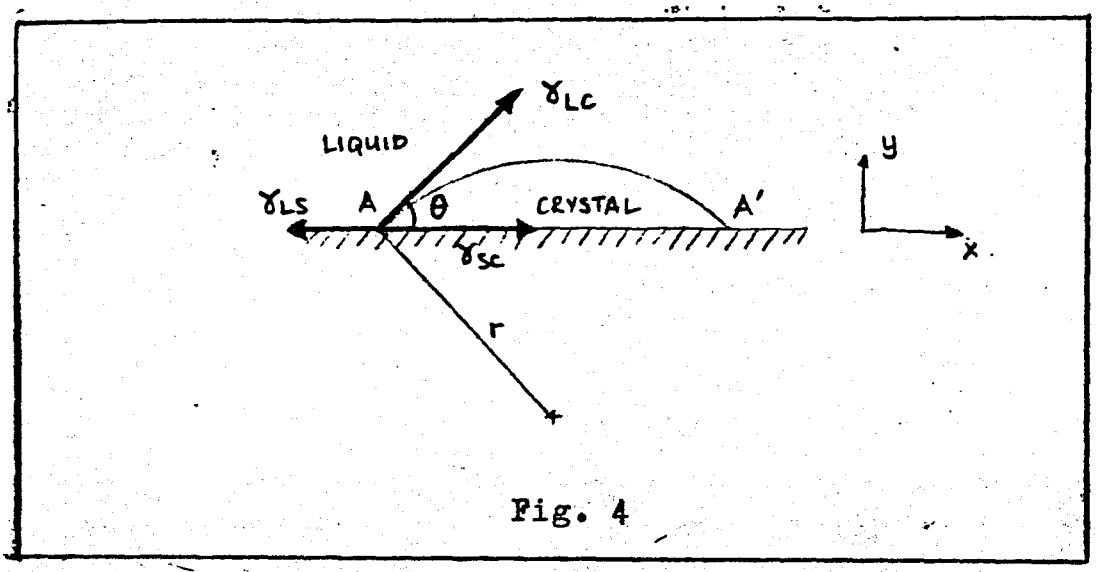

Fig. 4

where $\gamma_{SL}, \gamma_{SC}, \gamma_{LC}$ are the surface energies of substrate-liquid, substrate-crystal, liquid-crystal interfaces respectively.

The balance of horizantally resolved surface tensions require:

$$\gamma_{LS} = \gamma_{SC} + \gamma_{LC} \cos\theta \quad \text{----------} \quad (16)$$

where θ is the angle of contact.

In heterogenous nucleation, an additional term comes to the energy equation in Eq.4. For every square meter of growth of the substrate-cluster interface, there is a change in free energy equal to the difference between the interfacial energies of substrate-crystal and liquid-substrate:

$$\gamma_{SC} - \gamma_{LS} = -\gamma_{LC} \cos\theta \quad \text{----------} \quad (17)$$

The volume free energy term of heterogenous nucleation is:

$$\Sigma \Delta G_V = \Delta G_V V_{crystal} \quad \text{----------} \quad (18)$$

Total surface energy term is:

$$\Sigma \Delta G_S = \gamma_{LC} S_{LC} + (\gamma_{CS} - \gamma_{LS}) S_{CS} \quad \text{----------} \quad (19)$$

where S_{LC} and S_{CS} are the areas of liquid-crystal and crystal-substrate respectively.

$$\therefore \Delta G_{het}(r) = \Delta G_V V_S + \gamma_{LC} S_{LC} + (\gamma_{CS} - \gamma_{LS}) S_{CS} \quad \text{------} \quad (20)$$

Since

$$\left.\frac{d \Delta G^*_{het}}{dr}\right|_{r=r^*} = 0 \quad \text{----------} \quad (21)$$

and $$\Delta G^*_{het} = \Sigma \Delta G_{het}|_{r=r^*} \quad \text{----------} \quad (22)$$

It can be calculated from Eq.17,20 and 21 that:

$$\Delta G^{*}_{het}(r) = \frac{4}{3}\pi \gamma_{SL}^{3} \left\{ (2+\cos\theta)(1-\cos\theta)^{2} \right\} / \Delta G_{v}^{2} \quad \text{---(23)}$$

when

$\theta = 0^{\circ}$ $\Delta G^{*}_{het}(r) = 0$, complete wetting, no barrier to nucleation ---(24)

$$\theta = 90^{\circ} \quad \Delta G^{*}_{het}(r) = \frac{8}{3}\pi \frac{\gamma_{SL}^{3}}{\Delta G_{v}^{2}} \quad \text{----------(25)}$$

$$\theta = 180^{\circ} \quad \Delta G^{*}_{het}(r) = \frac{16}{3}\pi \frac{\gamma_{SL}^{3}}{\Delta G_{v}^{2}} \quad \text{----------(26)}$$

As seen from above calculations, as θ increases, nucleation barrier increases and reaches $\Delta G^{*}_{het} = \Delta G^{*}$ at $\theta = 180$.

2.2 Growth

Once nucleation occurs, crystal growth begins. For the growth to proceed, the number of atoms joining the lattice must be more than those leaving it. The undercooling required for the incorporation of atoms from the liquid into the solid is called "kinetic undercooling". The kinetic undercooling needed depends on the shape of the solid-liquid interface during growth. For a surface convex to the liquid, equilibrium melting temperature is lower then that of a flat surface; and this difference increases as the radius of curvature decreases. In pure metals, interface morphology is determined by the temperature gradient in the liquid at the solid-liquid interface. In alloys, the interface morphology is determined by the growth velocity, temperature gradient in the liquid at the solid-liquid interface and the purity level of the melt.

2.2.1 Growth in pure metals

During growth of pure metals, the temperature distribution in the melt can take several forms. When the temperature gradient in the liquid at the solid-liquid interface is positive, or zero(as seen in Fig.5a and 5b), growth proceeds with a planar interface.

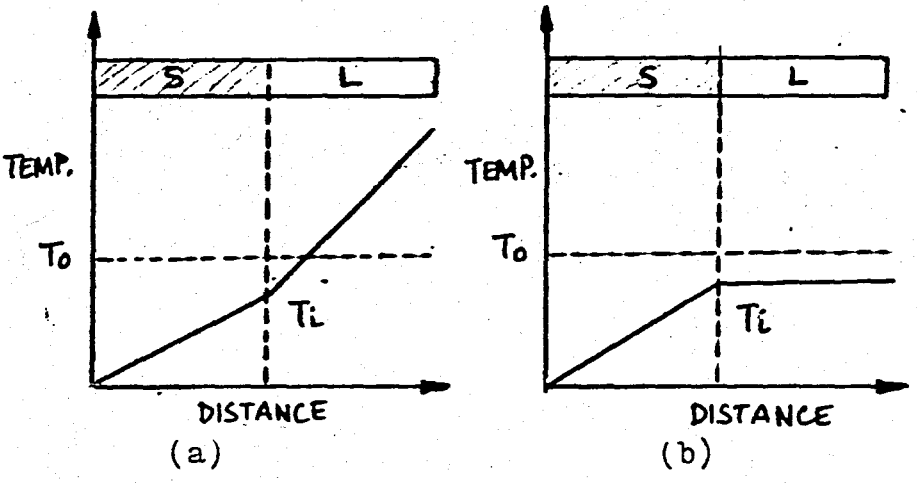

Fig.5

The reason for this can be understood by observing Fig.5. Assume that the temperature gradient is pdsitive, any perturbation which may occur on the planar interface will find itself in a region of higher temperature than the interface and will remelt.

When the temperature gradient in the liquid at the liquid-solid interface is negative, as seen in Fig.6, then the liquid ahead of the interface will be thermally undercooled.

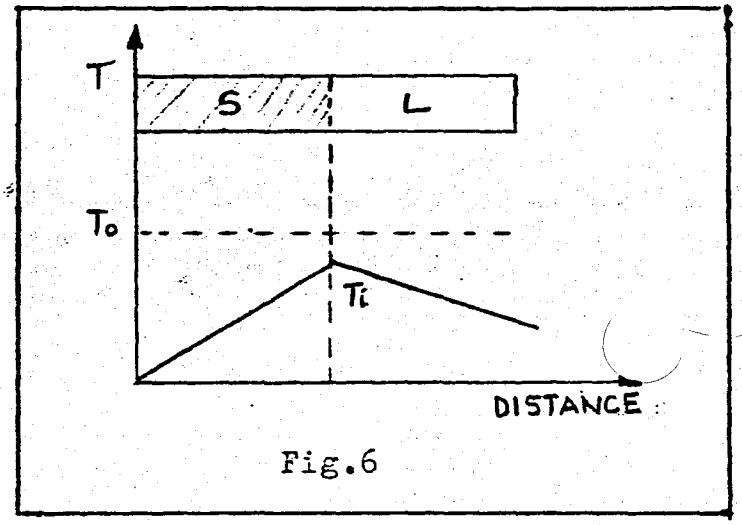

Fig.6

Then any perturbation forming at the interface will find itself in a region of greater undercooling than the interface. Therefore it will have a chance to grow at faster rate than the remainder of the interface. As a result, the interface breaks down and grows dendritically. Characteristic of dendritic growth is that the primary arms and side branches grow in definite crystallographic directions.[2]

Structure	Dendritic Growth Directions
fcc	⟨100⟩
bcc	⟨100⟩
hcp	⟨10$\bar{1}$0⟩
bct	⟨110⟩

2.2.2 Growth in Alloys

Consider a single crystal of alloy C_0 growing with a plane front.(Fig.7) Equilibrium at the solid-liquid interface can be attained at temperatures below the liquidus temperature T_L. If solidification is occuring at temperature T^*, the condition of equilibrium at the interface requires that the liquid and solid compositions at the interface C_L^* and C_S^*, respectively, be fixed by the phase diagram. Compositions away from the interface may be very different but the condition of equilibrium at the interface requires that if either T^*, C_L^* or C_S^* is specified, the other two are fixed by the phase diagram.

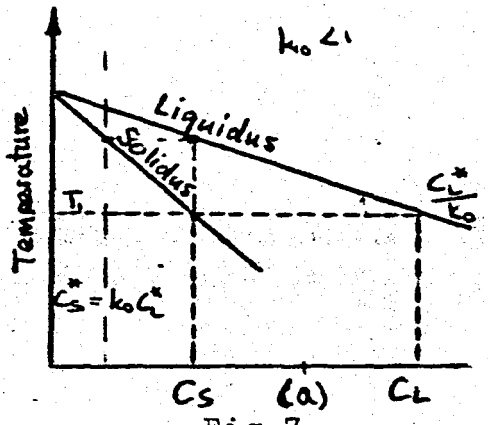

Fig.7

Phase diagram for the solidification of an alloy with equilibrium at the liquid-solid interface

In describing solidification under these conditions, it is convinient to define an equilibrium partition ratio k_0, where

$$k_0 = \frac{C_S^*}{C_L^*} \qquad (27)$$

k_0 may be either less than one or greater than one. When $k_0 < 1$, solute addition decreases the freezing point of the solid. This is a more common case than $k_0 > 1$, where the addition

of solute raises the freezing point of the solid. The composition of the forming solid and the interface morphology depends on the way in which the rejected solute or solvent is redistributed in the liquid ahead of the interface. When $k_o < 1$, solute is rejected by the solid as it forms; and when $k_o > 1$, solvent is rejected at the solid-liquid interface.

2.2.2.1 Solute Redistribution during Plane Front Solidification

When growth proceeds with a planar interface, the distribution profile of solute or solvent rejected at the liquid-solid interface may be considered for several different cases, with referance to "normal solidification process".[3] Normal solidification is the term used to describe solidification when an entire charge is melted and solidified with plane front from one end. This treatment assumes that:

a) Interface moves at a constant rate R

b) Compasition is uniform across any section parallel to the interface.

c) No significant undercooling occurs before nucleation.

d) Equilibrium distribution coefficient, k_o, is invariable with composition.

e) Liquidus slope, m, is constant.

f) Diffusivity of solute atoms in the liquid(D_L), is independent of concentration.

g) Equilibrium is achieved at all times at the solid-liquid interface.

Even though the following treatment applies for alloy systems where $k_o < 1$, it is also applicable for $k_o > 1$.

(i) Equilibrium solidification occurs only if the freezing rate is slow enough to permit the diffusion process in the solid and liquid to erase any concentration gradients, i.e. complete diffusion in the liquid state and complete diffusion in the solid state.

Let us consider the solidification of an alloy of initial concentration C_o. Solidification begins when the temperature reaches T_L, equilibrium liquidus temperature. The composition of the first forming solid is $k_o C_o$. Since $k_o < 1$, solute is rejected into the liquid from the liquid-solid interface.(Fig.8a)

During subsequent cooling and solidification, both the liquid and solid become enriched in solute; at temperature T^*, the solid of composition C_S^* is forming in equilibrium at the liquid-solid interface with liquid of composition C_L^*. Because diffusion in the solid and liquid is complete, the entire solid becomes of uniform composition, $C_S = C_S^*$, and the entire liquid of uniform composition $C_L = C_L^*$. (Fig.8b) At temperature T^*, a general materials balance is written:

$$C_S f_S + C_L f_L = C_o \qquad (28)$$

where f_S and f_L are weight fractions of solid and liquid, respectively.

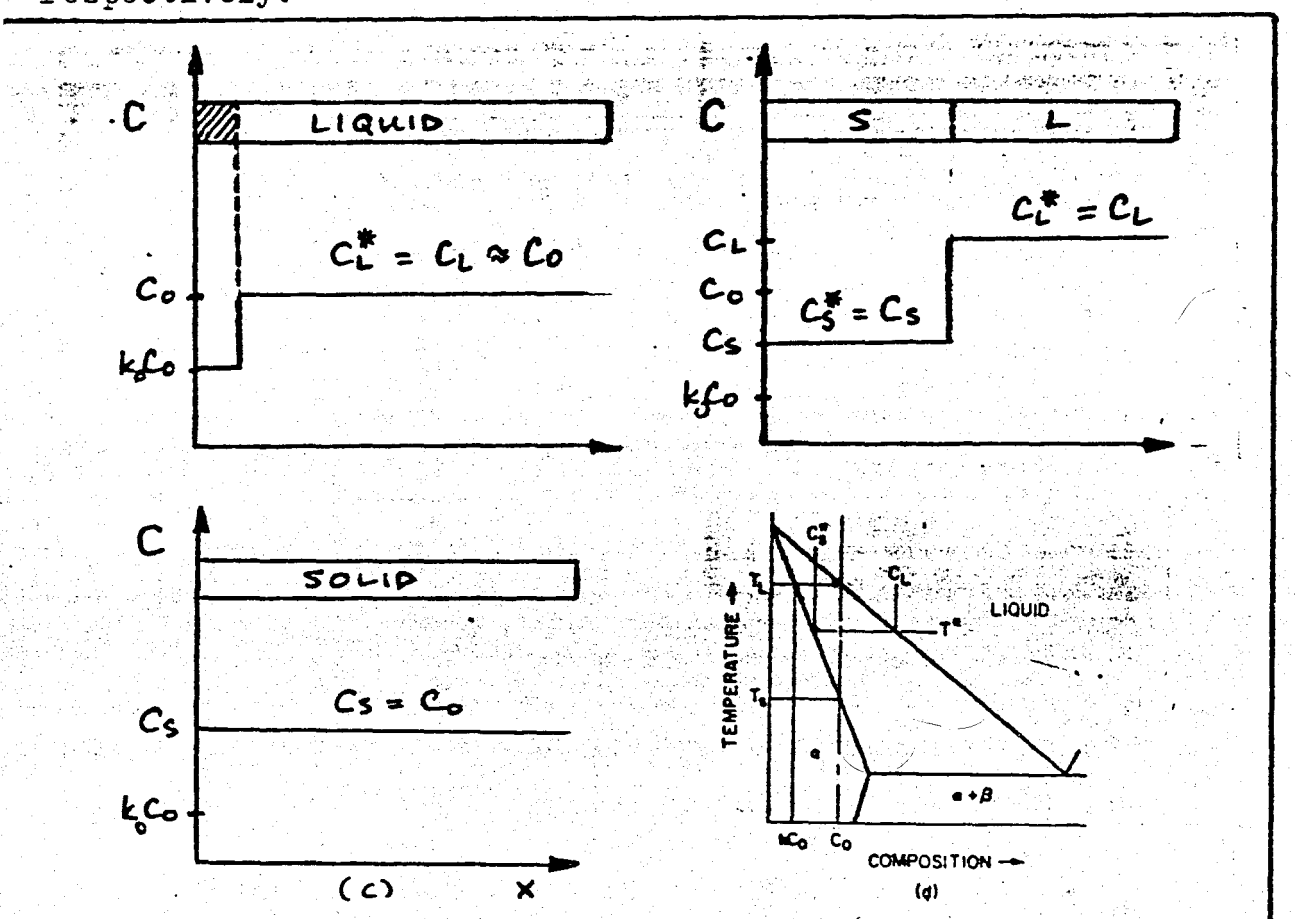

Fig.8

Equilibrium freezing of an alloy with initial concentration C_o
a) Solute redistribution at T_L b) Solute redistribution at T^*
c) Solute redistribution at T_S^* d) Part of the phase diagram

Since:

$$f_s + f_L = 1 \quad \text{----------} \quad (29)$$

Eq.28 can be readily solved for fraction solidified at a given temperature.

At complete solidification, balance may be obtained as below: Considering Eq.29 and 27; Eq.28 may be rewritten as:

$$f_s C_s^* + (1 - f_s)\frac{C_s^*}{k_o} = C_o \quad \text{----------} \quad (30)$$

At complete solidification no fraction of liquid remains, i.e. $f_L = 0$. Then, from Eq.29, $f_s = 1$. Eq.30 takes up the form:

$$C_s^* + (1 - 1)\frac{C_s^*}{k_o} = C_o \quad \text{----------} \quad (31)$$

$$C_s^* = C_o \quad \text{----------} \quad (32)$$

(ii) Complete mixing in the liquid, no solid diffusion

A melt of initial composition C_o begins to solidify as the temperature falls to T_L. As in equilibrium solidification, the first small amount of solid to form has the composition $k_o C_o$ at temperature T_L.

During subsequent cooling and solidification, the liquid becomes richer in solute and so the solid that forms is of higher solute content at later stages of solidification. Since there is no diffusion in the solid state, the composition of the solid formed at the initial stages of freezing remains unchanged. At temperature T^*, solid of composition C_s^* is freezing from liquid of composition C_L^* and the solute distribution along the length of growing crystal is as shown in Fig.9. A quantitative expression is obtained by equating solute rejected when a small amount of solid with the resultant solute increase in the liquid. This balance is:

$$(C_L - C_s^*)\, df_s = (1 - f_s)\, dC_L \quad \text{----------} \quad (33)$$

where f_s = fraction of material solidified.

Substituting the equilibrium partition ratio and integrating from $C_s^* = k_o C_o$ at $f_s = 0$ yields the composition of the solid at the liquid-solid interface C_s^* as a function of solid fraction:

$$C_s^* = k_o C_o (1 - f_s)^{(k_o - 1)} \quad \text{----------} \quad (34)$$

or in terms of liquid composition and fraction of liquid:

$$C_L^* = C_0 f_L^{(k_0-1)} \qquad \text{.....(35)}$$

Eq.34 and Eq.35 are termed nonequilibrium lever rule. These equations closely describe solute redistribution in crystal growth under a wide range of experimental conditions.

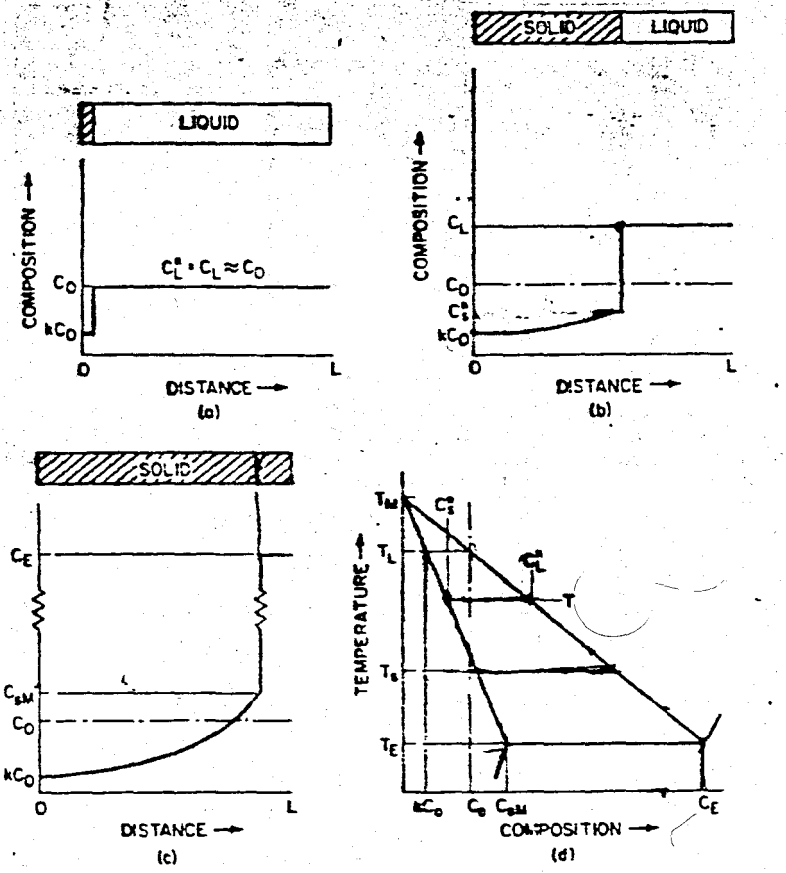

Fig.9

Solute redistribution in solidification with no solid diffusion and complete diffusion in liquid. a)At the start of solidification b)At temperature T^* c)After solidification d)Phase diagram

(iii) No solid diffusion, transport in liquid by diffusion only.

As before, solidification begins with the formation of a solid of composition $k_o C_o$. Soon a solute diffusion boundary layer develops ahead of the interface. If the crystal is sufficiently long, steady state is approached, as sketched in Fig.10a

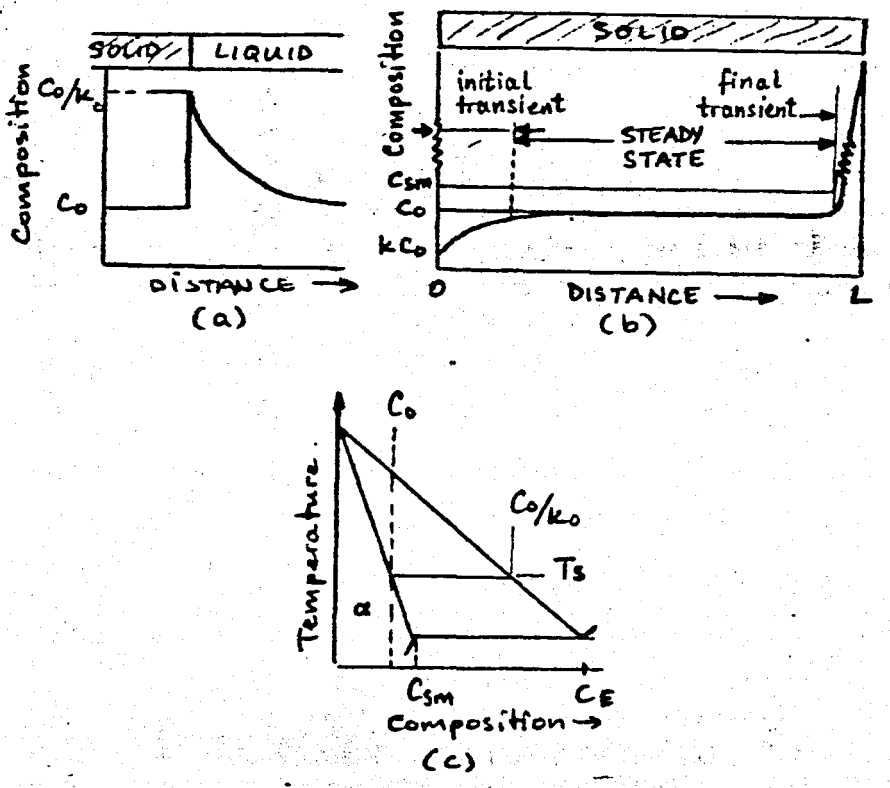

Fig.10

Solute redistribution in solidification with limited liquid diffusion and no convection. a) Composition profile during steady state solidification b) Composition profile after solidification c) Phase diagram

At this steady state, the composition of the solid forming is exactly of initial composition C_o. Equilibrium at the interface then requires that the composition of the liquid at the interface be C_o/k_o and solidification to occur at solidus temperature T_s. The solute distribution in the boundary layer in the steady state region is given by the differential equation: [4], [5]

$$D_L \frac{d^2 C_L}{dx'^2} + R \frac{dC_L}{dx'} = 0 \qquad \text{---------- (36)}$$

where x' is the distance from the interface into the liquid
D_L is the diffusion coefficient of solute in the liquid
R is the rate of movement of the interface

Boundary conditions are:

$$C_L = C_o / k_o \quad \text{at} \quad x' = 0$$
$$C_L = C_o \quad \text{at} \quad x' = \infty$$

Also, the requirement of solute conservation at the interface gives directly the gradient of composition in the liquid at the interface:

$$\left(\frac{dC_L}{dx'}\right)_{x'=0} = -\frac{R}{D_L} C_L^* (1 - k_o) \qquad (37)$$

Then solution to Eq.36 can be obtained by the aid of Eq.37; as:

$$C_L = C_o \left(1 + \frac{1-k_o}{k_o} e^{-(R/D_L)x'}\right) \qquad (38)$$

Here, the quantity D_L/R may be considered a characteristic distance, the distance at which the quantity $C_L - C_o$ falls to 1/e of the maximum $C_o/k_o - C_o$.

Solidification processes of this type results in a crystal of nearly uniform composition, except for the initial and final transients, as shown in Fig.10b.

The initial transient is formed while the solute boundary layer builds up to its maximum steady state value. Solute redistribution during initial transient can be obtained using the time dependent form of Eq.36:

$$\frac{\partial C_L}{\partial t} = D_L \frac{\partial^2 C_L}{\partial x'^2} + R \frac{\partial C_L}{\partial x'} \qquad (39)$$

where t is time.

The conservation equation(Eq.37) applies here as in steady state solidification, and the boundary conditions for the initial transient are:

$$C_L = C_o \quad \text{at} \quad t = 0 \quad \text{for} \quad x' > 0$$
$$C_L = C_o \quad \text{at} \quad t > 0 \quad \text{for} \quad x' = \infty$$

The solution for this equation for small values of k_0 is:

$$C_S^* = C_0 \left[1 - (1-k_0)\, e^{-(k_0 R x / D_L)} \right] \quad \text{----------(40).}$$

and

$$C_L^* = C_0 \left\{ \frac{1-k_0}{k_0} \left[1 - \exp\left(-k_0 \frac{R^2}{D_L} t\right) \right] \exp\left(\frac{-R}{D_L} x' \right) + 1 \right\} \quad \text{----(41)}$$

Then the characteristic distance for the length of this transient is D_L/Rk_0 . At this distance, the composition of the solid forming has risen to 1-(1/e) of its maximum.

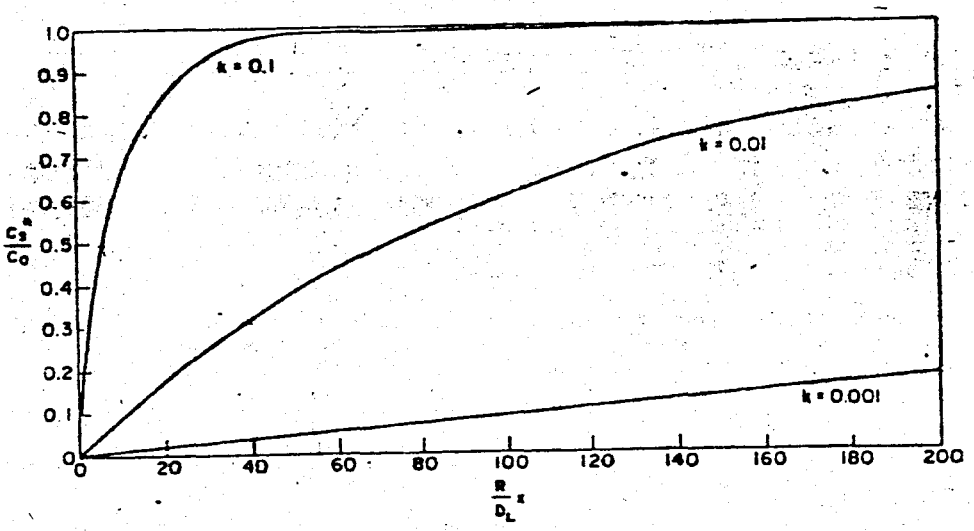

Fig.11
Solute redistribution in initial transient (Ref.5)

The final transient is much smaller than the initial transient since it results from the impingement of the solute boundary layer on the extremity of the crucible. Once the steady state has been achieved, it will be maintained as long as there is sufficient liquid ahead of the interface for the forward diffusion of the solute to occur without hinderence, and as long as the growth rate remains constant. The former condition ceases to be satisfied when the boundary of the liquid is approached and the concentration of the solid that is formed begins to rise above C_0 in order to accomodate the excess solute which may all appear in the terminal region. The length of the transient zone is the order of the characteristic distance of the solute boundary layer, or D_L/R. Fig.10b shows a schematic representation of this final transient. Solute concentration in final transient rises from C_0 to C_E at the ingot

2.2.2.1.1 The Effect of Changing R

Knowing the characteristics of the solute distribution in both the liquid and the solid, it can be understood that increasing or decreasing the speed of growth produces transverse bands of higher or lower concentration. C_L is given by Eq.38 for any growth rate R. When R is constant, the amount of solute carried forward ahead of the interface is proportional to characteristic distance D_L/R and is inversely proportional to the rate of solidification R.

If growth rate is increased, exponential curve gets steeper. The characteristic distance is less for the increased growth velocity. Thus, the excess solute that was initially in the boundary layer must appear as a solute rich band in the vicinity of the region where velocity change has occured. When the distribution comes again to steady state at a new growth rate, the concentration at the interface must again be C_o/k_o. If R decreases, the amount of solute entering the solid is temporarily reduced.

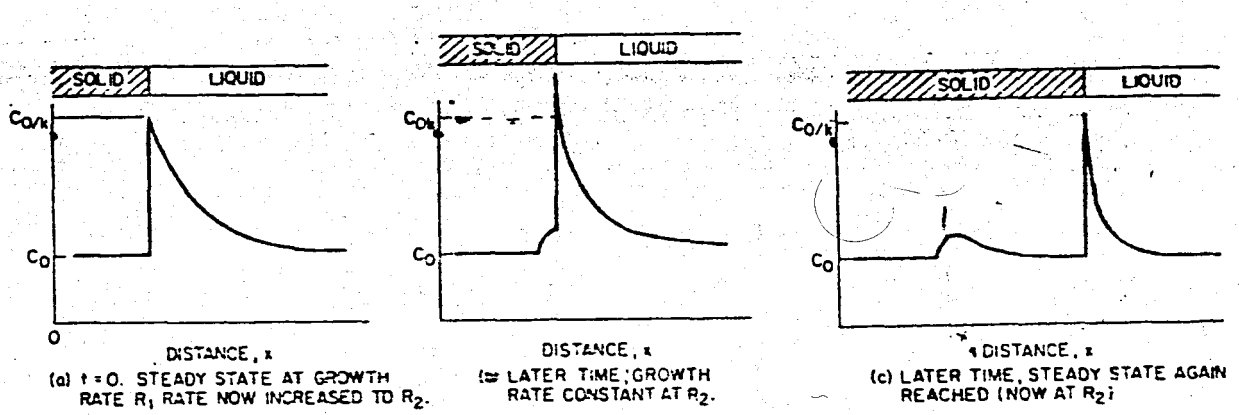

Fig.12
Solute-rich band resulting from increase in solidification velocity.

2.2.2.1.2 Effect of Convection

In most real cases of crystal growth, some convection is present. The solute redistribution in these cases has been treated by various workers.[7],[6] Burton, Primm and Slichter[7] treated the problem as follows: A diffusion boundary layer of thickness δ is assumed, outside which liquid composition is maintained uniform by convection and inside which mass transport is by diffusion only. (Fig.13)

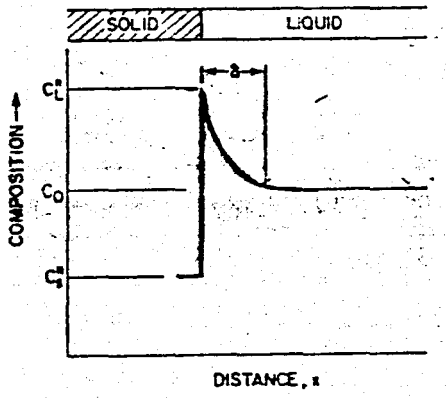

Fig.13
Solute profile in the liquid for solidification with convection

If solidification is taking place in a very large liquid bath, the bulk liquid composition is not altered by the solid forming and remains constant at C_0. At steady state:

$$(C_{bulk} - C_s)R + D_L \frac{dC}{dx} = 0 \quad \text{at } x' = 0 \qquad \text{----------(42)}$$

and the differential equation(Eq.36) applies with the boundary conditions:

$$C_L = C_L^* \quad \text{at} \quad x' = 0$$
$$C_L = C_0 \quad \text{at} \quad x' = \delta$$

Thus at interface:

$$\frac{C_L^* - C_S^*}{C_{bulk} - C_S^*} = e^{R\delta/D_L} \qquad \text{----------(43)}$$

For convenience, an effective partition ratio, k_E, which is the solid composition forming C_S^* divided by the bulk liquid composition is defined. Substituting in Eq.43:

$$k_E = \frac{k_o}{k_o + (1 - k_o)\, e^{-(R\delta/D_L)}} \qquad (44)$$

This expression may be used to describe solute redistribution in crucibles of finite length, provided that the thickness of the boundary layer is small compared to the length of the crucible. When this condition is satisfied, a dynamic equilibrium is attained between the bulk melt and growing solid and equations identical to Eq.34 may be derived; only now k_o is replaced by k_E ; to obtain "normal segregation equation":

$$C_S^* = k_E\, C_{bulk}\, (1 - f_S)^{k_E - 1} \qquad (45)$$

$$C_L = C_{bulk}\, f_L^{k_E - 1} \qquad (46)$$

here, C_L is the bulk liquid composition and $k_E = C_S^* / C_L$

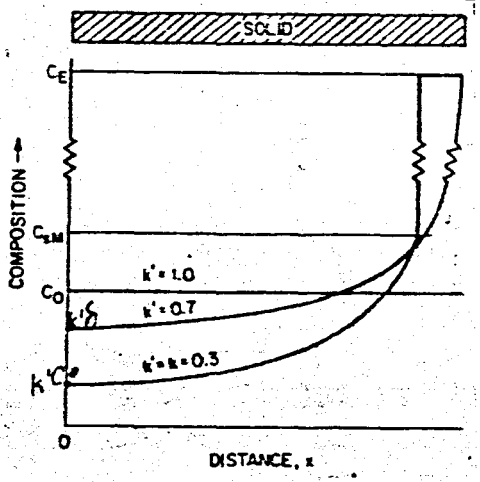

Fig.14
Final solute distribution for solidification with limited liquid diffusion and various amounts of convection

Fig.14 shows some calculations of solute for the alloy of precceding examples, taking $k_E = k_o$, unity and an arbitrary value between the minimum(k_o) and maximum(1). As seen from Eq.43, the minimum value occurs when $R\delta/D_L \ll 1$, i.e. at slow growth rate, high diffusivity and maximum stirring. The maximum value of k_E (equal to unity) is obtained for $R\delta/D_L \gg 1$. Under these conditions, any convection present has negligible effect on solute distribution.

2.2.2.2 Instability of the Planar Interface

In real cases of crystal growth, the liquid in contact with a planar liquid-solid interface generally has a composition that differs from the bulk liquid composition. As a result, the equilibrium liquidus temperature of the liquid in contact with the interface is lower than that of the liquid away from the interface. (Fig.15)

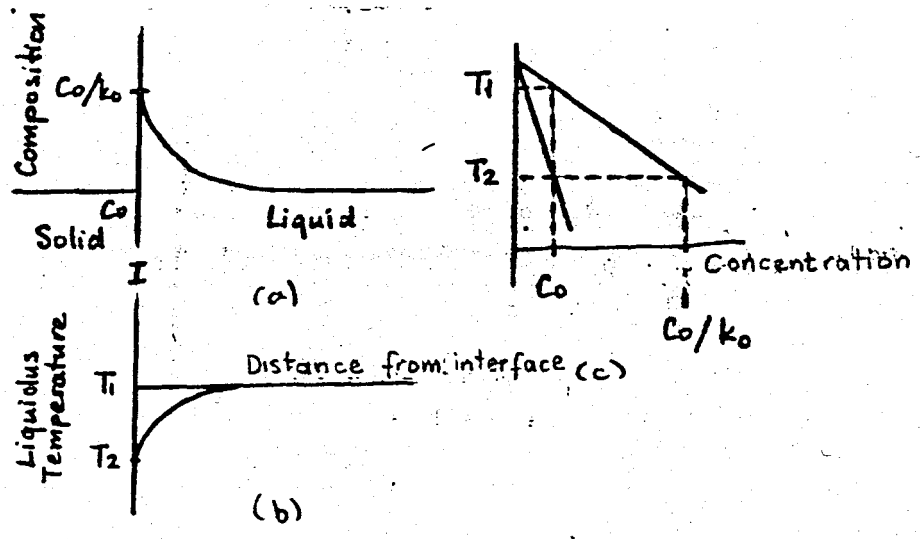

Fig.15
Variation of concentration and liquidus temperature ahead of the interface. a)Variation of concentration b)Relationship between concentration and liquidus temperature c)Variation of liquidus temperature.

In such cases, the interface morphology is determined by the actual temperature distribution in the liquid at the interface, G_L. If G_L is lower than the gradient of the equilibrium liquidus temperature at the interface, then a volume of liquid ahead of the interface will be "constitutionally supercooled."[8] (Fig.16)

Consequently, a planar interface will be unstable since the growth rate will be increased in any localized region that advanced ahead of the general interface. The projection continues to grow by rejecting solute or solvent laterally and longitudinally until a steady state growth condition is reached.

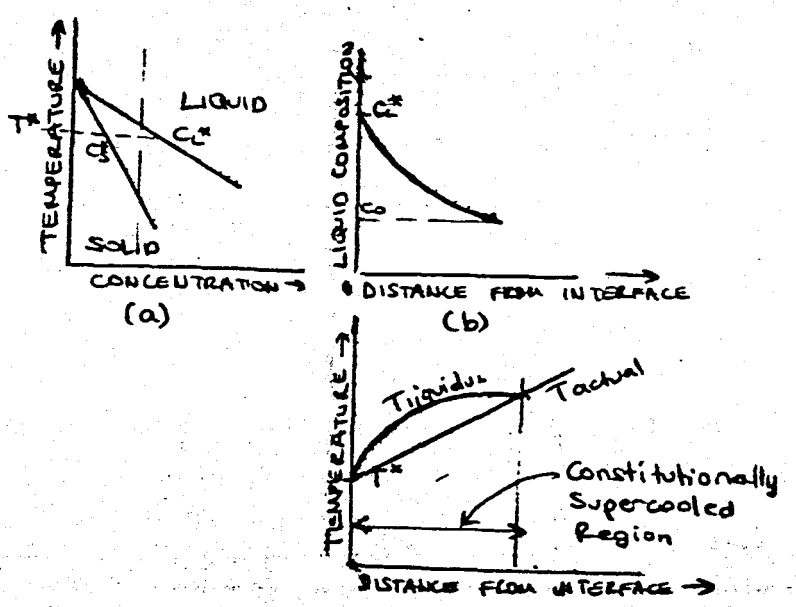

Fig.16
Constitutional supercooling of liquid ahead of a planar liquid-solid interface; a)Part of the phase diagram b)Solute redistribution c)Constitutionally supercooled region

Assuming steady state planar growth conditions, the extend of constitutional supercooling and the length of constitutionally supercooled zone can be calculated.[41] The solute distribution was given in Eq.38. The equilibrium temperature T_E may be obtained from the equilibrium diagram as:

$$T_E = T_o - m_L C_L \qquad (47)$$

where T_o = melting point of the pure metal
m_L = slope of the liquidus line, assumed constant.

Thus the equilibrium temperature at any point at the interface is given by:

$$T_E = T_o - m_L C_o \left[1 + \frac{1-k_o}{k_o} \exp\left(-\frac{R}{D_L} x'\right)\right] \qquad (48)$$

Actual temperature ahead of the interface may be expressed as:

$$T = T_o - m_L \frac{C_o}{k_o} + G_L x' \qquad (49)$$

where $T_o - m_L C_o/k_o$ is the temperature at the interface and G_L is the temperature gradient in the liquid.

Constitutional supercooling is existant when:

$$\left.\frac{dT_L}{dx'}\right|_{x'=0} < \frac{dT_{actual}}{dx'} \qquad \text{---------- (50)}$$

and the extend of constitutionally supercooled zone is the point of intersection other than $x'=0$.

Thus for $T = T_E$:

$$1 - \exp\left(-\frac{R}{D_L}x'\right) = \frac{G_L}{m_L C_o\left(\frac{1-k_o}{k_o}\right)}x' \qquad \text{---------- (51)}$$

By Eq,50 and Eq.51, it can be shown that constitutional supercooling is existant only when:

$$\frac{G_L}{R} < -\frac{m_L C_o}{D_L}\cdot\frac{(1-k_o)}{k_o} \qquad \text{---------- (52)}$$

Instability of the planar interface leads eventually to the development of dendritic growth. The transition structure is cellular.

For crystals growing into stirred melts,[9] the conditions for stability may be found using the same reasoning:

$$\frac{G_L}{R} \geq -\frac{m_L C_{bulk}(1-k_o)}{D_L\left[k_o + (1-k_o)\exp(-R\delta/D_L)\right]} \qquad \text{---------- (53)}$$

for very efficient mixing, as $R\delta/D_L$ approaches zero, stability condition may be expressed as:

$$\frac{G_L}{R} \geq \frac{m_L C_o(1-k_o)}{D_L} \qquad \text{---------- (54)}$$

Instability develops initially to cellular morphology which then transforms into dendritic structure.

2.2.2.3 Cellular Growth

The nature and growth conditions of cellular substructure has been investigated in detail.[4],[7],[8],[9],[10],[11] These structures are columnar in the direction of growth and hexagonal in cross section, with the cell boundaries being richer in solute in comparison with the cell centers.

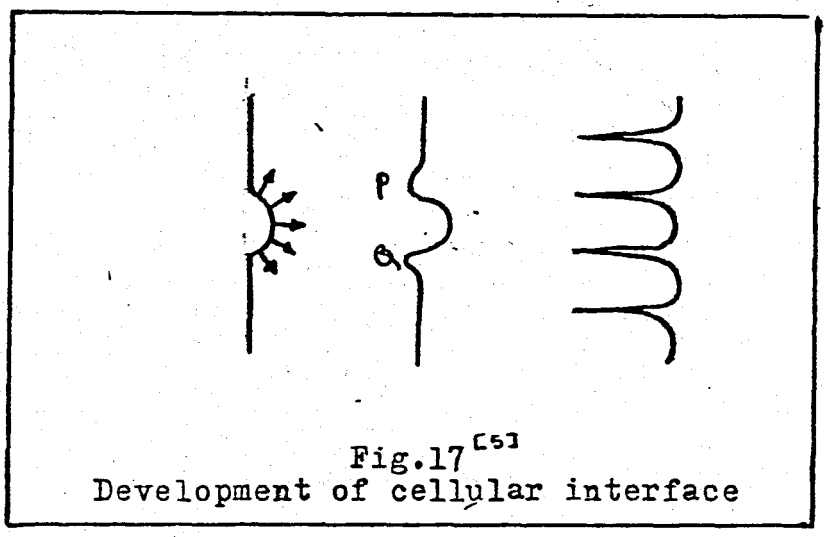

Fig.17[5]
Development of cellular interface

Experiments on transparent organic liquids have shown[11] that a planar interface first becomes gently undulatory when it becomes unstable, then the protrusions later develop into fully formed cells. The accumulation of solute around the base of the perturbance retards solidification in this region and consequently perturbance can not expand laterally. The convexity caused thereby in regions such as P and Q in Fig.17 triggers the development of similar proturbances around the original one and the result is an array of cells which have approximately "closed packed" structure, most cells having six neighbors.

As growth conditions depart from those required for plane front a number of transition structures were observed before well developed hexagonal cells.[11],[12] The structures obtained depends also on crystallographic directions. With Pb-Sn alloys[12] it was observed that in the crystal growing in <110>direction, elongated cells developed with the segregate concentrated in the planar intercellular regions. In the crystal growing in <100> direction, the segregate was found to be concentrated in roughly cylindrical regions termed nodes. The liquid-solid interface for the two orientations discussed above is shown schematically in Fig.18. These structures are metallographic sections of solidified specimens.

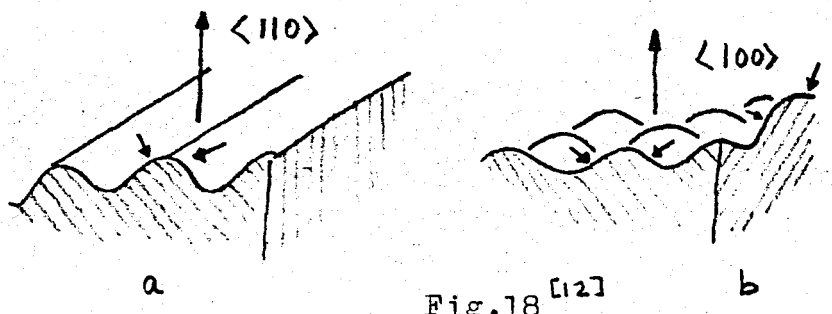

Fig.18 [12]

Schematic representation of developing perturbations for two solid-liquid interface orientations a)<110> growth direction (elongated cells developed) b)<100> growth direction (nodes developed) The relative locations of regions near a {111} on the perturbations are shown by short arrows.

An alternative way of studying cellular structures is to decant the bulk liquid during solidification.[13],[14] An example of a structure obtained in this way is shown in Fig.19.

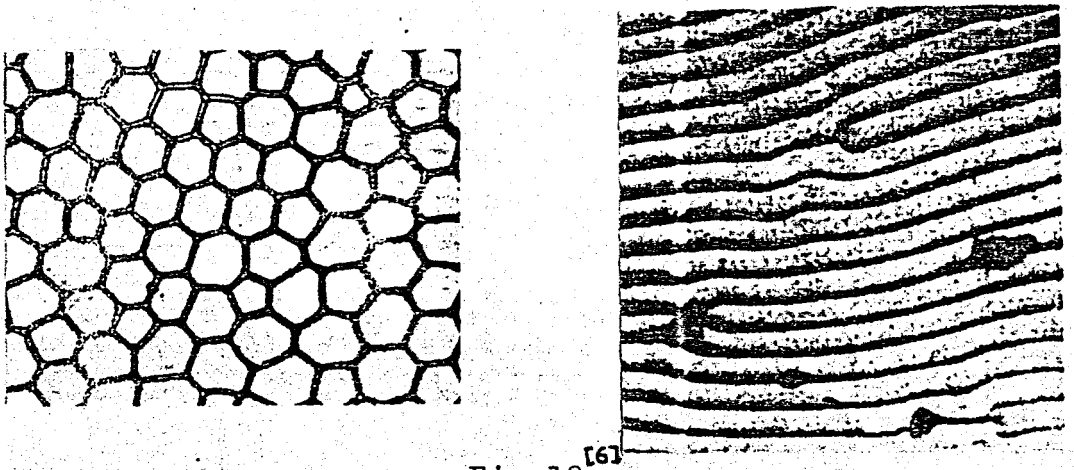

Fig.19 [6]

Decanted interface of cellularly solidified Pb-Sn alloys

In germanium crystals, during development of cellular structure, the interface was first found to be smoothly rippled and subsequent development of facets were observed when portions of the interface reached the orientation of a {111} plane.

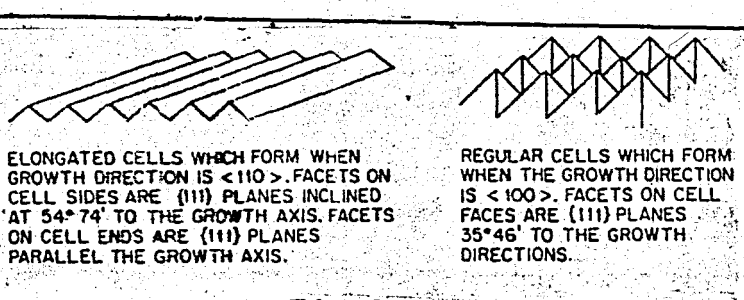

Fig.20

Schematic illustration of cell morphology in germanium alloys.

A probable explanation of this growth characteristic is given as:[6] In the case of ⟨100⟩ growth direction in cubic metals, a perturbation on the interface will have four symmetrically placed regions of {111} orientation; for this is the closest packed plane and is expected to be slowest growing. Thus, these four slow growing regions "guide" the shape of perturbation to be of roughly equal dimensions transverse to the heat flow direction. The relatively small amount of segregate in dilute alloys with high G_L/R then concentrations in the lowest positions of the interface as nodes. In the case of {110} oriented crystal, a perturbation will have two such slow growing planes, guiding the interface morphology to a furrowed structure and leading to elongated cells.

Various studies have been done to test whether the breakdown of planar interface into a cellular one occurs at the onset constitutional supercooling ahead of the planar interface.[10],[15] [16],[17],[18],[19]. For growth into quiescent melts, at steady state, breakdown was found to occur at a critical value of G_L/R for a given solute concentration C_o as predicted by the criterion of Eq.52. Two typical examples are shown in Fig.21 and Fig.22

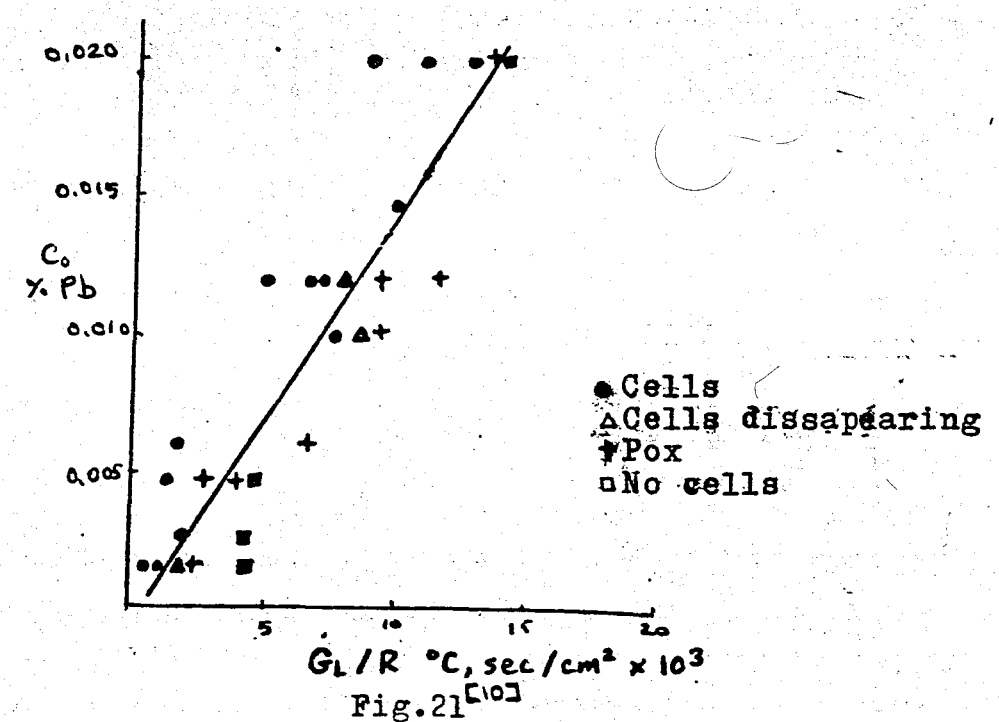

Fig.21[10]

Results for Pb-Sn, plotted as C_o vs. G_L/R for cell formation

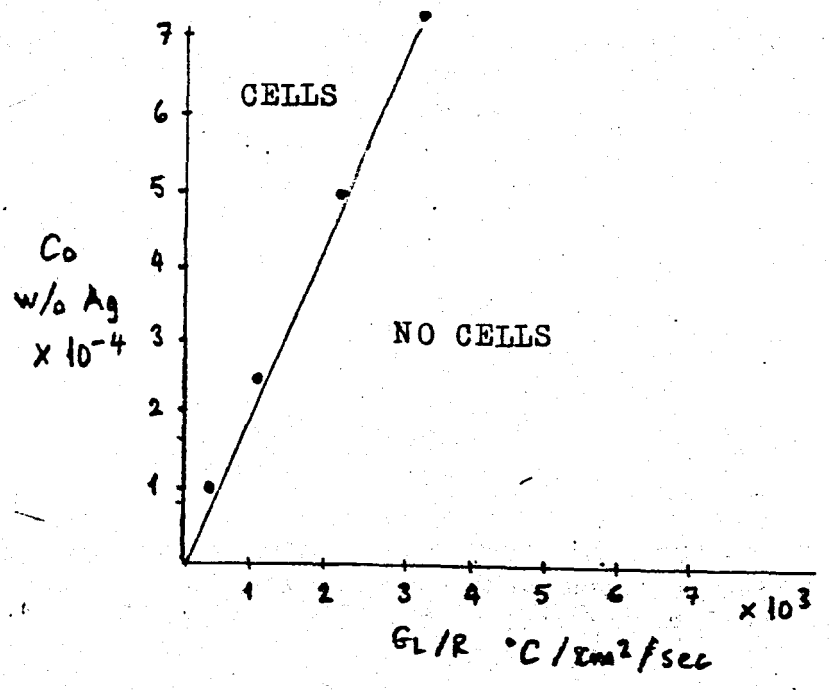

Fig.22[17]

Results for Pb-Ag alloys, plotted as C_0 vs. G_L/R for cell formation.

For growth into stirred melts, the actual temperature gradient in the liquid just ahead of the interface is calculated by the condition of conservation of heat flux in the interface[18]:

$$k_L G_L = k_S G_S - L\rho R \qquad (55)$$

where L = Latent heat of solid

K_L, K_S = Thermal conductivity of liquid and solid respectively

ρ = Density of the solvent

Constitutional supercooling will be avoided if the actual temperature gradient in the liquid is equal to, or greater than the equilibrium liquidus temperature, i.e.:

$$\left.\frac{dT_E}{dx}\right|_{x=0} = G_L \qquad (56)$$

Using Eq.55 and Eq,56:

$$\frac{k_S G_S - L\rho R}{k_L} = \frac{-m_L R C_L (1-k_o)}{D\{k_o + (1-k_o)\exp(-R\delta/D_L)\}} \qquad (57)$$

The effect of the solute distribution is to give a gradient of supercooling(dS/dx) away from the interface. The magnitude

of the effect can be expressed by $(dS/dx)\big|_{x=0}$ which is:

$$\left(\frac{dS}{dx}\right)\Big|_{x=0} = -\frac{m_L R C_L (1-k_o)}{D_L\{k_o + (1-k_o)\exp(-R\delta/D_L)} - \frac{k_s G_s - L\rho R}{k_L} \quad (58)$$

where $d = 1.6 D_L^{1/3} \nu^{1/6} \omega^{-1/2}$

ν = kinematic viscosity of melt

ω = stirring rate

$(dS/dx)_{x=0}$ increases as R increases.

Expressed in the terms of C_S , Eq.58 becomes:

$$\frac{dS}{dx}\Big|_{x=0} = \frac{m_L R C_S}{D_L}\frac{(1-k_o)}{k_o} - \frac{k_s G_s - L\rho R}{k_L} \quad \text{----------(59)}$$

which is independent of stirring rate.

Assuming a fixed, critical value of supercooling at the interface is required to initiate cell formation, then at slow growth rates Eq.59 may be rewritten as:

$$\ln C_3 = -\ln R + \ln \frac{D_L}{p'}\left\{\left(\frac{ds}{dx}\right)_{x=0} C_r + \frac{k_s G_s}{k_L}\right. \quad \text{----------(60)}$$

for alloys with constant $p' = \frac{-m_L(1-k_o)}{k_o}$

When p' is variable,

$$\ln C_s p' = \ln R + \ln D_L\left\{\left(\frac{dS}{dx}\right)_{x=0} C_r + \frac{k_s G_s}{k_L}\right\} \quad \text{--------(61)}$$

Accordingly, the plots of both Eq.60 and Eq.61 is expected to give straight lines with slopes of -1. Experimental results agree with teory.[12][15] Two examples of experimental varification are shown in Fig.23 and 24.

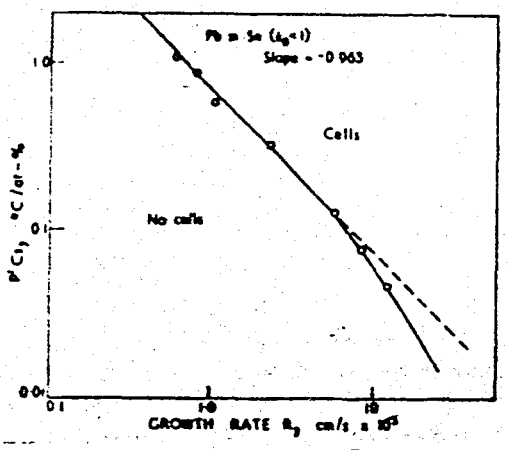

Fig.23 [15]

Conditions for planar-cellular transition in Sn-Pb alloys

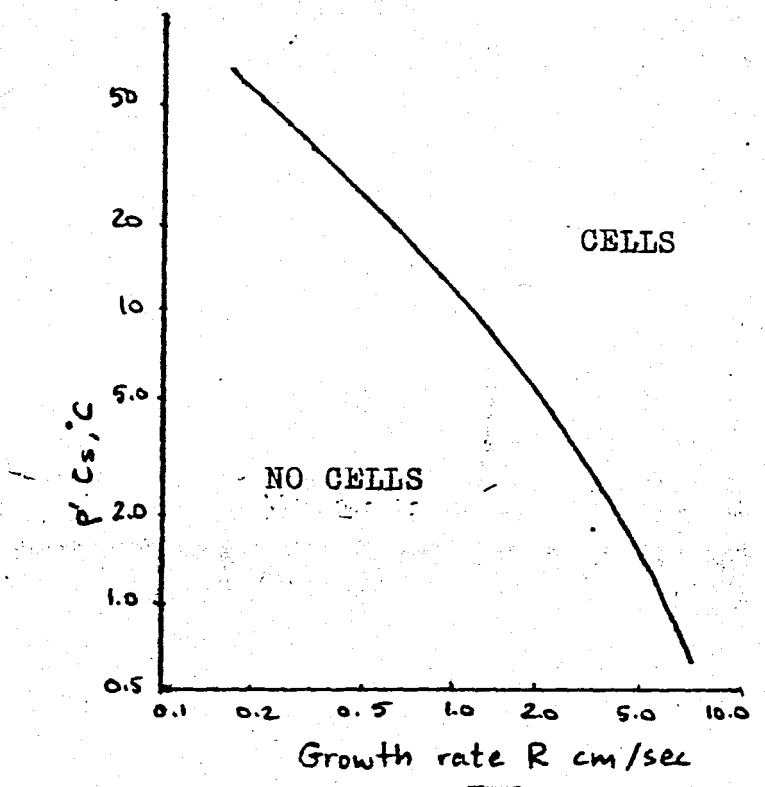

Fig.24 [12]

Graph of p'C for which cellular growth commenced as a function of growth rate R.

Attempts have been made to test the constitutional supercooling criteria quantitatively, by comparing the D_L values which are obtained by Eq.52,60 and 61 with those measured experimentally. The results are shown in Table I. It can be observed that whether k_o is greater or less than unity, D_L values estimated by constitutional supercooling criterion agrees well with the experimental results.

Table I

A comparison between D_L values obtained through constitutional supercooling criteria and those obtained by direct measurements.

Solvent	Solute	D_L by C.S. criteria $cm^2/sec \times 10^{-5}$	D_L measured $cm^2/sec \times 10^{-5}$	Reference
Sn	Pb	1.7	2.1	10
Pb	Sn	7.2	1.7	17
Pb	Ag	5.4	-	17
Sn	Pb	7.6	2.1	16
Sn	Bi	9.1	0.9	16
Al	Cu	3.0	-	18

2.2.2.4 Cellular/Dendritic Growth

During cellular growth, if the temperature gradient is reduced and/or rate of growth is increased, dendritic structure developes. The steps of transformation are illustrated in Fig.25 [12]

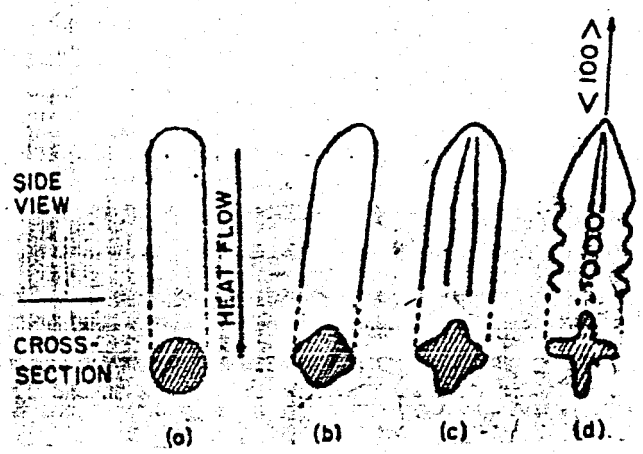

Fig.25[12]
Sketch of the changing shape of growth structure as growth velocity is increased. a)Regular cell growing at low velocity b)Regular cell growing in <100> dendrite direction c)Flanged cell d)Dendrite exibiting the start of perioric lateral branching

The transition is orientation dependent, when <100> and <110> are near the direction of heat flow, the cells join to form almost continuous parallel plates rather than a row of individual dendrites. Near a <111>, periodic sidebranches form rather than a continuous flange, and the transition starts at this direction first. Chalmers[5] introduced the term "cellular-dendrite" for the type which has characteristic cell tips with square pyramidal shape and form a square array to differentiate it from the more rod-like branched dendrites observed during free dendritic growth of undercooled melts.

Various attemps have been made to establish a relationship between the growth conditions and cellular/dendritic transition. The earliest one was that of Tiller and Rutter.[17] These workers studied a series of lead crystals containing tin concentrations ranging from 0.25-2.0% by weight. According to the experimental results, C_o vs. $G_L/R^{1/2}$ was graphed.(Fig.26) and a relation was found in the form of:

$$A_o C_o = G_L / R^{1/2} \qquad (62)$$

where A_o = a constant for a particular growth direction

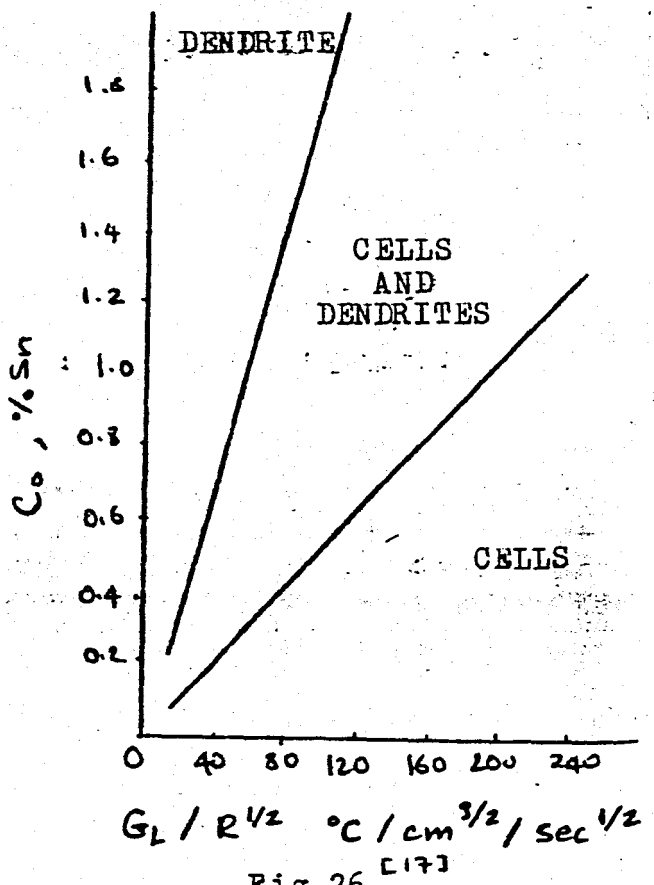

Fig.26 [17]

Growth conditions for cellular/dendritic transition

Holmes et.al.[20] found results in good agreement with that of Tiller and Rutter.(Fig.27) They proposed that the cellular/dendritic transition is dependent upon the quantity of solute in the liquid at the interface prior to the breakdown of planar interface.

On the other hand, the results reached by Plaskett and Winegard[16] disagreed with the above two calculations. Working with Sn-Pb, Sn-Bi, Sn-Sb they observed that the transition from cells to dendrites when plotted as $G_L/R^{1/2}$ vs. C_o/k_o was not linear and showed no dependence on orientation.(Fig.28) However, they observed that a linear relationship is possible for the plots of:

$$d_t \frac{C_o}{k_o} \quad \text{vs.} \quad A \frac{G_L}{R^{1/2}} \qquad \text{----------(63)}$$

where d_t = cell size at transition
A = a constant

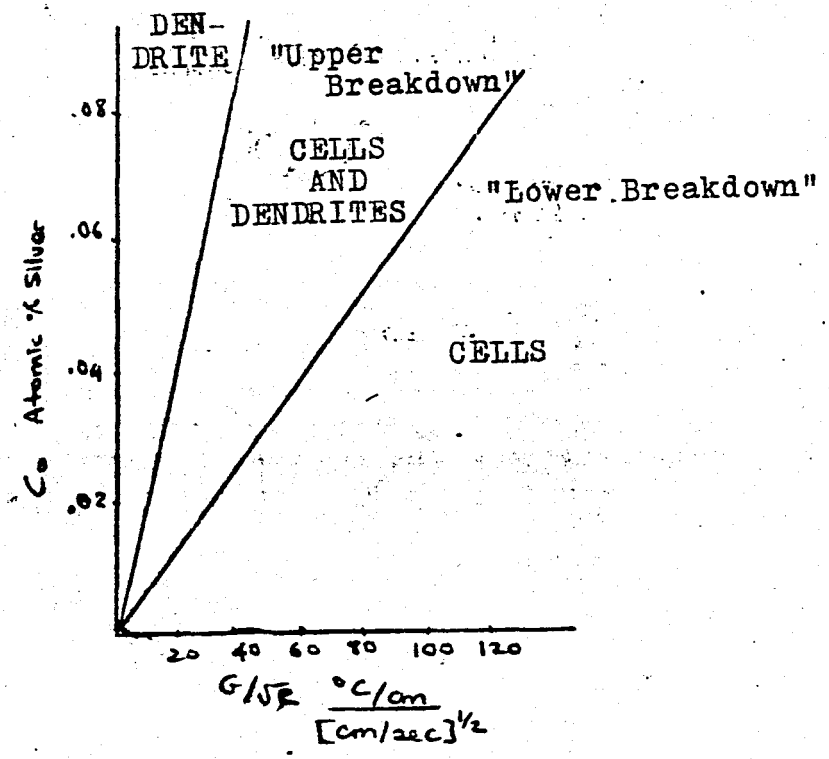

Fig.27 [20]
Cell/dendrite transition (Ag as a solute in Pb).

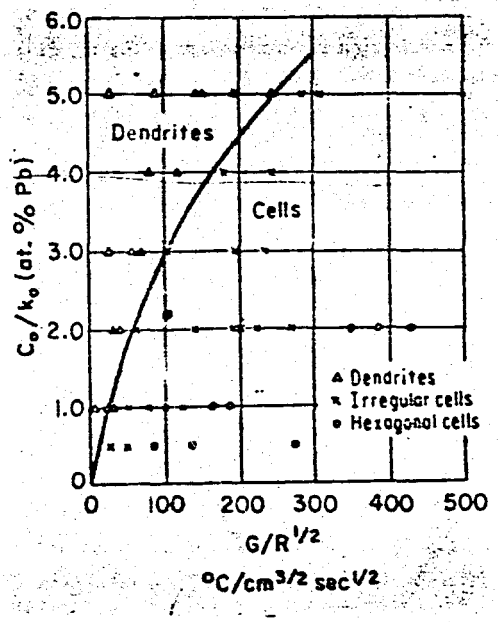

Fig.28 [16]
Growing conditions for cell/dendrite transition in Sn-Pb alloys

No theoretical justification was given in developing Eq.63, Recent measurements of Coulthard and Elliott [21] have not been able to varify this relation. These workers concluded that both G_L/R and $G_L/R^{1/2}$ give curved results when used with C_o/k_o to define cellular/cellular-dendritic transition as seen in Fig.29,30 and 31; and suggested a relationship in the general form:

$$d_t^n \frac{C_o}{k_o} \propto \frac{G_L}{R} \qquad \text{---------- (64)}$$

for the prediction of the transition. Here, d_t is the cell size at transition for a grain of orientation t.

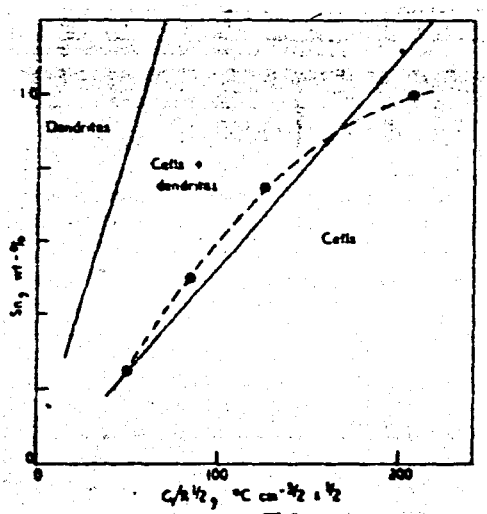

Fig.29 [21]

Dotted curve drawn by Coulthard and Elliott as a possible curve

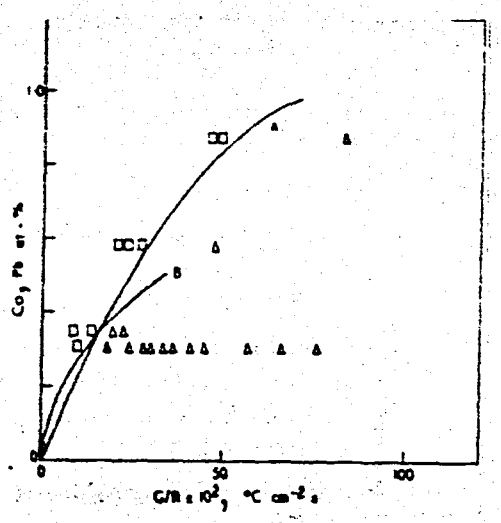

Fig.30 [21]

The relationship between C_o and $G_L/R^{1/2}$ for Sn-Pb alloys. Curve A is Coulthard and Elliot's; B is Plaskett and Winegard's.

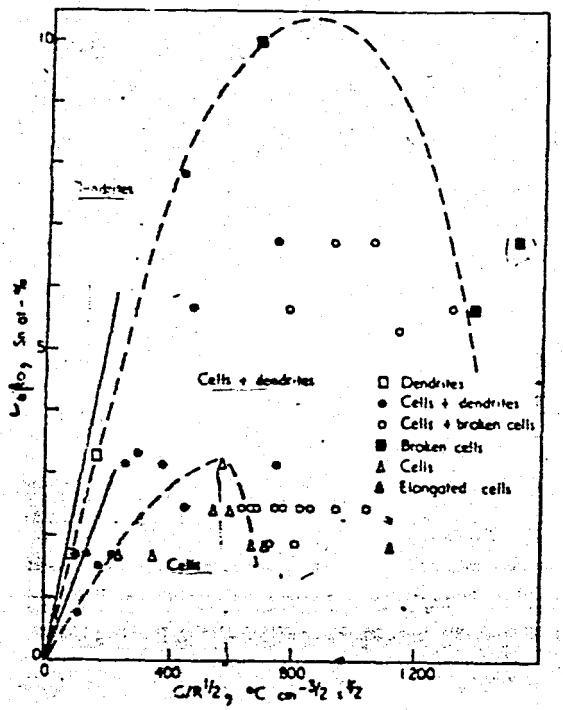

Fig.3 [21]

The relationship between C_o/k_o and $G_L/R^{1/2}$ for the Pb-Sn system. Full lines are Tiller and Rutter graph.

Even though the arguments continue about the criteria of cellular/dendritic transition, it is clear that reduced temperature gradients in the liquid and increased growth rate and solute contents (i.e. conditions which produce increased constitutional supercooling) favor the cellular/dendritic transition.

2.3 Aspects of Dendritic Growth

Conditions that lead to well developed cellular or cellular/dendritic morphologies also lead to severe segregation of solute or solvent to the cell walls or interdendritic regions. [8],[22],[23],[24] Consequently, the tip temperature of dendrites is greater than that of the planar interface from which dendrites develop. The dendrite tip temperature may be defined as:

$$T_t = T_L - \Delta T_k - \Delta T_R - \Delta T_s \qquad (65)$$

where ΔT_k = kinetic undercooling

ΔT_R = curvature undercooling

ΔT_s = solute undercooling

everal theoretical treatments of dendrite tip temperature are vailable. A particular one is that of Kramer, Bolling and Tiller.[24] he workers defined the effective distribution at the tip, k_E^t s:

$$k_E^t = -\frac{k_o}{m_L C_o}\Delta T \qquad (66)$$

here $\Delta T = T_m - T_a$

T_m = melting point of the pure solvent

T_a = actual temperature at the tip of the cell

nd observed that k_E^t approaches k_o for lower values of G_L/RC_o nd increases towards unity at higher values of this parameter. harp and Hellawell obtained similar results with their study.

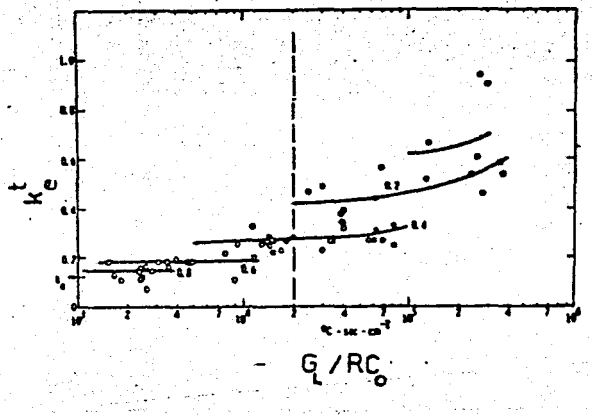

Fig.32[24]

ramer et.al. results for measured relationship between cellu- ar/dendrite tip temperature and growth conditions. (Sn-Pb)

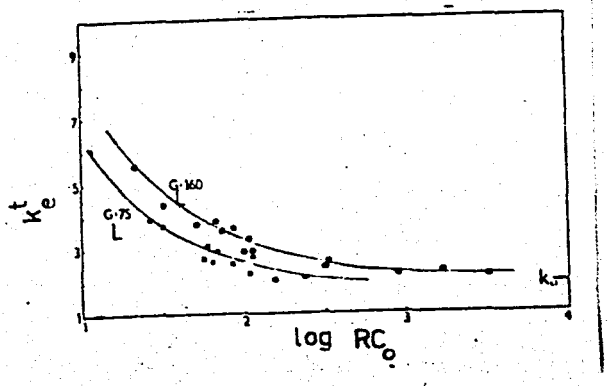

Fig.33

Results for Al-Cu alloy.

On the other hand, Backerud and Chalmers[25] have shown evidence by temperature measurements of some remaining constitutional supercooling at the dendrite tips in the ingot castings of Al-Cu alloys. They also demonstrated that, assuming zero gradiant in the liquid ahead of the interface, solute undercooling at the dendrite tips increase with increasing R and C_0 .(Fig.34)

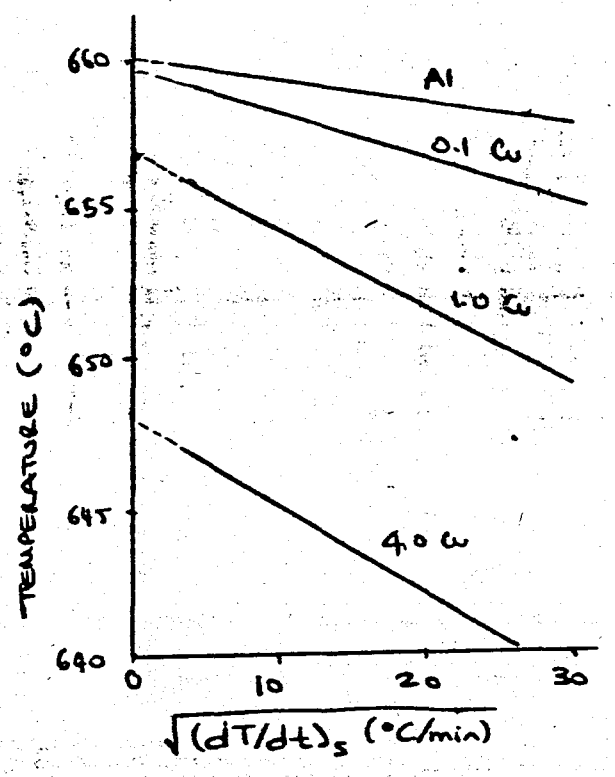

Fig.34
Measured relationship between dendrite tip temperature and growth conditions during ingot solidification

Burden and Hunt[26] made a clarifying study in Al-Cu systems and concluded that at high temperature gradients and low velocities the tip temperature increases with increasing velocity, but for high enough velocities the temperature decreases with increasing velocity and then becomes independent of the gradient. For a zero gradient, the interface temperature decreases from liquidus temperature for increasing growth rate. The undercooling increases with increasing solute content.

Burden and Hunt explain the inconsistencies of previous workers to be due to the effect of temperature gradient. Although high

temperature gradients were present in the work of Kramer et.al. and Sharp and Hellawell, they were not present in the work of Backerud and Chalmers and Doherty and Feest. Fig.35 illustrates the results of Burden and Hunt vs. the results of Backerud and Chalmers. Fig.36 illustrates the measured relationship between dendrite tip temperature and growth conditions during unidirectional solidification for an Al-Cu system.

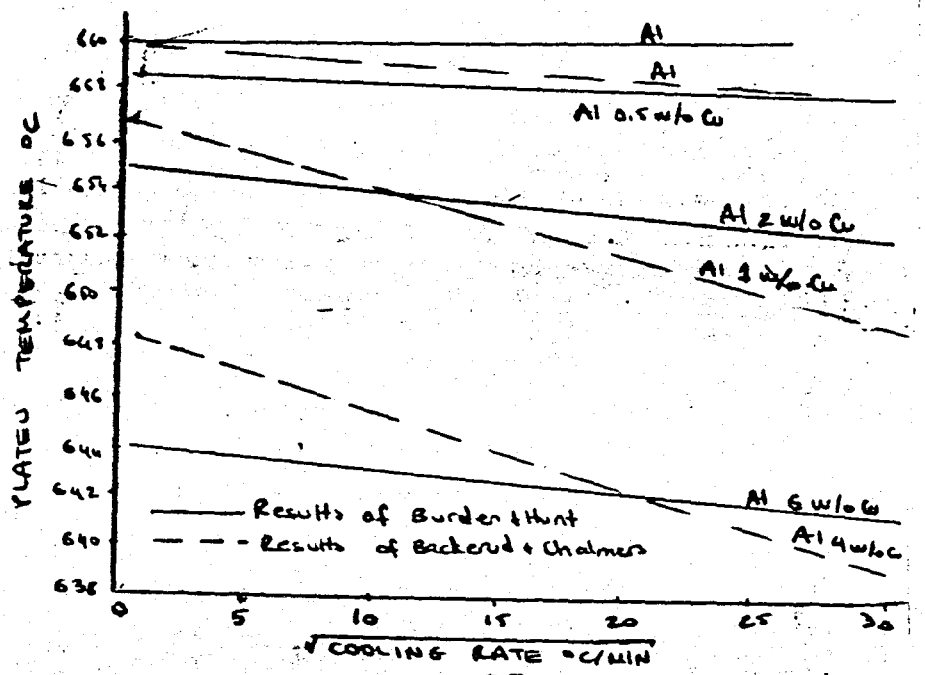

Fig.35 [26]

Variation of plateu temperature for pure Al and Al-Cu alloys

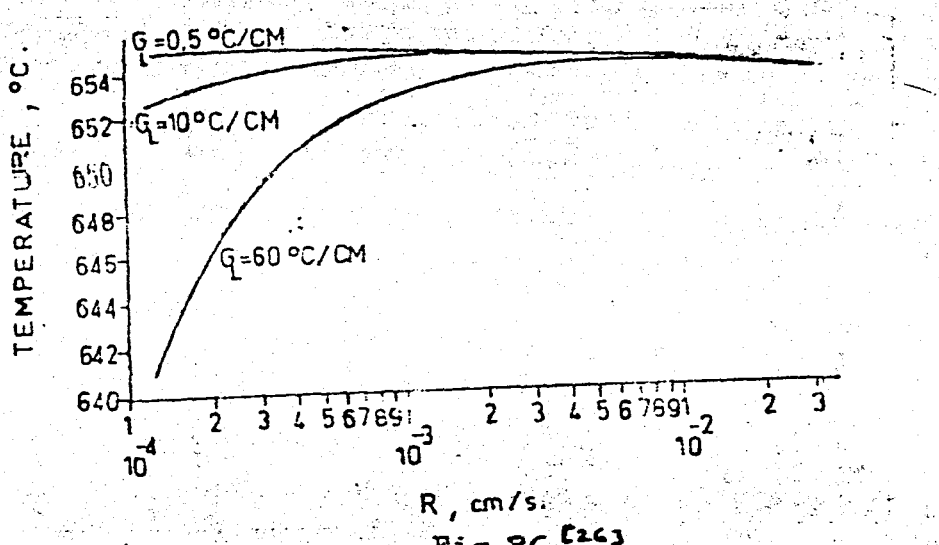

Fig.36 [26]

Measured relationship between dendrite tip temperature and growth conditions during unidirectional solidification of Al-Cu

2.3.I Dendrite Growth Models

After it was demonstrated that dendrites represent the most advanced stage of interfacial instability in a wide class of materials, a multiplicity of theories arose attempting to describe dendritic growth.

The steady state dendritic heat transfer problem is to be solved in the solid and liquid regions subject to two boundary conditions at the surface of the dendrite:[27]

1) Temperature at each point on the solid-liquid interface equals the local equilibrium freezing temperature which is determined by the local interface curvature κ.

2) The latent heat released at the interface during solidification is constantly conducted away through the adjoining solid and liquid phases.

However, both conditions are incompletely defined since the capillary condition as well as the normal component of the temperature gradient in the energy conservation condition must be calculated from the dendrite geometry. The shape of the dendrite is not known a priori, and must be determined as part of the solution to the diffusion problem. To eliminate the nonlinear aspects of this free boundary problem, the boundary conditions given above were usually simplified or dendrite shapes predetermined by assumption. In the first dendritic growth models, branching of the dendrite was ignored and dendrites were assumed to be paraboloidal needles without branches, which grew at a constant rate and in a shape preserving manner.[1][28],[29][30] The tip speed was assumed to reach a maximum for a given undercooling. This maximum speed that is assumed to control dendritic growth is given by Ivantsov as:[25]

$$V_{max} = \frac{2\alpha\Omega}{\rho} \qquad (67)$$

where α = thermal diffusivity of liquid

Ω = a constant depending on bath supercooling and thermal properties of liquid and solid

ρ = radius of curvature of dendrite tip

The modified Ivantsov and Temkin models also yield similar results in the form of:[Ref.27]

$$\Delta\theta = P\acute{e}\, e^{P\acute{e}} E_1(P\acute{e}) + \Delta\theta_c \qquad (68)$$

where $\Delta\theta = \frac{\Delta T C_p}{L}$; dimensionless supercooling

$C_p =$ heat capacity of the liquid phase

$L =$ heat of fusion

$E_1(P\acute{e}) =$ exponential integral function ($\int_{P\acute{e}}^{\infty} (e^{-u}/u)\,du$)

$P\acute{e} = VR/2\alpha$ Péclet number at the dendrite tip

$R =$ dendrite tip radius

$\Delta\theta_c =$ a term reflecting the influence of capillary (Gibbs-Thomson) effect and is a function of V and R.

Equation 68 reflects two major physical effects. The point effect (VR: constant) is the solution to the thermal diffusion model with an isothermal interface, in which $\gamma = 0$ is assumed and consequently $\Delta\theta_c = 0$. On the other hand, if $\gamma \neq 0$, then the Gibbs-Thomson effect lowers the interface equilibrium temperature by $T_m\gamma K/L$ which effectively reduces by the same amount the supercooling available to "drive" the thermal diffusion. This reduction in supercooling prevents dendrites growing increasingly fast as R approaches zero, as would be required by the point effect. Generally, capillary limited theory in the form of Eq.68 only limits the growth velocity to being no larger than an upper bound value of $V(V_{max})$ at a given supercooling $\Delta\theta$. Unique relationships for V vs. $\Delta\theta$ and R vs. $\Delta\theta$ are therefore lacking in these models. Glicksman et. al.[11] performed experiments to test these these theories and found that the results do not fit the theoretical calculations: (Fig.37)

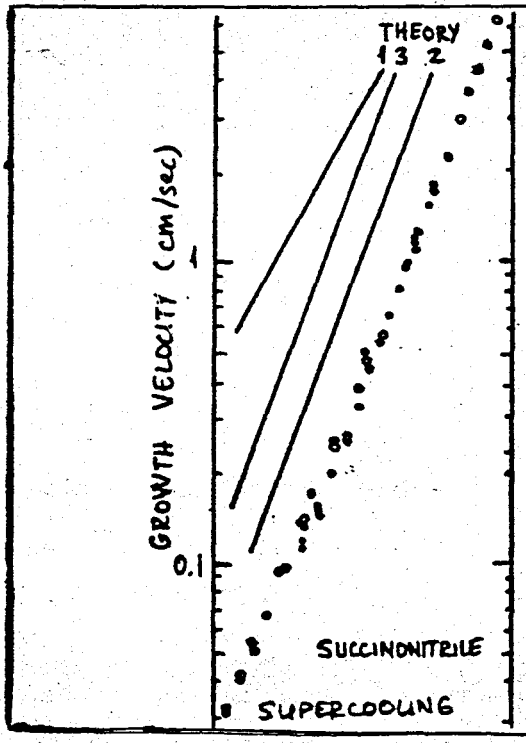

Fig.37[11]

Free dendritic growth vs. supercooling

Theory I-Ivantsov

Theory 2-Trivedi

Theory 3-Nash and Glicksman

In later studies,[31][32] it was observed that the basis solution (the optimized Temkin needle dendrite) used in these analyses was incorrect since the optimized Temkin dendrite does not have large perturbations near the tip and has perturbations only away from the tip, contrary to that of a real dendrite. In search of a new needle dendrite, Oldfield[31] recognized the need for the dendrite tip to achieve a stable condition so that its steady state growth could be ensured. According to this hypothesis the basis dendrite for branching stability analysis should be the one with the stable tip. Based on this concept, several stability criteria for dendrite tips have been developed:

i) Oldfield's model: The stable size of a dendrite tip is determined, based on the idea that the destabilizing force due to thermal diffusion is equal to the stabilizing capillary force. The temperature gradient in front of a dendrite tip propagating at a steady velocity V can be expressed as:[31]

$$G_{L,tip} = -\frac{LV}{\alpha C_p} \qquad (69)$$

where $G_{L,\xi}$ = temperature gradient normal to the dendrite tip

And the stability criterion is stated as:

$$\sigma^* = 2\alpha d_0 / VR^2 = 0.02 \qquad (70)$$

where σ^* = stability criterion constant

d_0 = capillary length defined as $T_m \gamma C_p / L^2$

ii) Planar interface model: In this model[28][29] the dendrite tip is first considered to be a point lying on a planar interface which propagates at the axial dendritic growth velocity, V (Fig. 3

According to Mullins and Sekerka, for a crystal with a planar interface to grow stably, the wavelength of perturbation must remain smaller than

$$\lambda_s = 2\pi\sqrt{2\alpha d_0 / V} \qquad (71)$$

where λ_s critical perturbation wavelength

Relating λ_s to the size of dendrite tip such that

$$R \simeq \lambda_s \qquad (72)$$

Then the criterion of Eq.71 becomes

$$\sigma_s = 2\alpha d_o / VR^2 = \frac{1}{4\pi^2} = 0.0253 \quad \text{-----------} \quad (73)$$

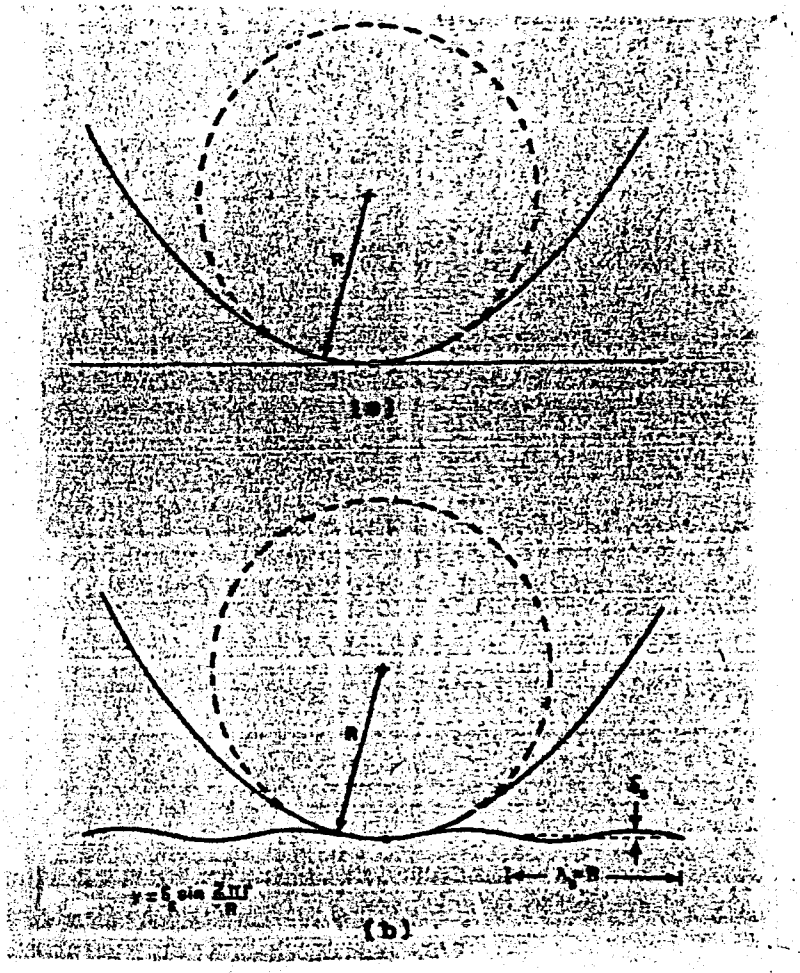

Fig.38
Schematic showing the planar interface model for estimating dendrite tip stability:a)before perturbation is considered b)the marginally stable condition,at which $\lambda_s = R$ and $\delta_s = \sigma^* \lambda_s$

iii)Spherical model:In this model, the stability criterion of the dendrite tip is assumed to be identical to that of a sphere which describes the local total curvature of the dendrite tip 2/R. Since the growth of a sphere is a nonsteady state problem, to simulate the steady state growth of the dendrite tip, steady state conditions must be imposed on the growing sphere. The absolute stability condition for a growing sphere with an instantaneous radius R has been given [ec.7] by:

$$G_{L,sphere} = \frac{T_m \gamma}{LR^2}(n+2)(2n+1) \quad \text{-----------} \quad (74)$$

where n = spherical harmonics order

Under the mentioned "steady-state" condition, the temperature gradient around the sphere is equal to $LV/\alpha Cp$. Then Eq.74 becomes

$$\sigma^* = 2\alpha d_0 / VR^2 = \frac{2}{(n+2)(2n+1)} \quad \text{----------(75)}$$

Selecting $n=6\cong 2\pi$ to be consistent with the assumption used in the planar model that the dendritic tip radius approximates the perturbation wavelength, Eq.75 takes up the form

$$\sigma^* = 2\alpha d_0 / VR^2 = 0.0192 \quad \text{----------(76)}$$

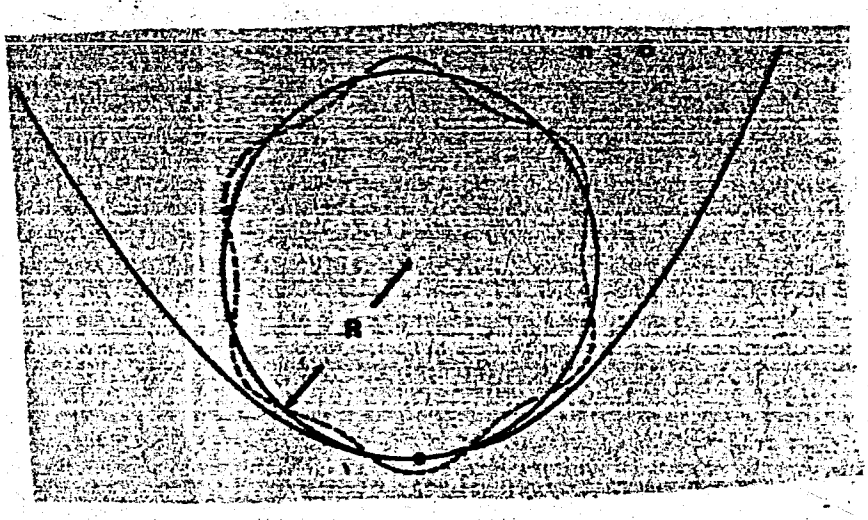

Fig.39
Schematic showing the spherical interface model at a marginal stability condition with harmonics $n=6$ but $\delta \neq 0$.

iv)Langer and Müller-Krumbhaar(LM-K)[32] theory:In this theory, rigorous mathematics and an extensive numerical computation were used to study the interface behavior of the whole dendrite The procedure used by LM-K started with the derivation of a linear integro-differential equation to describe the displacement of the dendrite surface away from the unperturbed base paraboloid. The equation of motion was derived making a quasi-stationary approximation for the time dependent diffusion field. Also in the derivation,thermal diffusion in the solid phase was neglected and perfect material isotropy assumed. At the limit Pé$\rightarrow$0, an equation of motion was obtained which contains the stability parameter σ as the only system-dependent quantity. The equation of motion had no exact solution when $\sigma \neq 0$ and was studied numerically by an eigenvalue analysis.

If the dendrite shape displacement had an exponential time-dependence, then the eigenstate found was such that when

$$\sigma^* = 2\alpha d_0 / VR^2 = 0.025 \pm 0.007 \quad \text{----------} (77)$$

all the unstable modes at the dendrite tip vanished.

Huang and Glicksman[7] performed experiments to determine the validity of the above stated theories and concluded that:
1)A complete steady state dendritic growth theory should in the main include both the heat transfer and consideration of dendrite tip stability.
2)Ivantsov's simple solution to dendritic heat transfer problem is substantially correct. Accordingly, the capillary effects must be trivial since dendrites grow with tip dimensions about 100 times larger than the critical radius for nucleation. Also, the assumption of a needle dendrite shape seems consistent with the experimentally observed axial growth kinetics at the tip.
3)The stability criteria developed in several models assuming VR^2 = constant agrees with the measurements.

The above conclusions are reached for free dendritic growth. J.D.Hunt[33] made an analysis to put forward an expression to describe the growth process in alloys and commercially pure materials which freeze with a cellular or dendrite growth front. Assuming a cell or dendrite tip may be approximated by a smooth steady state shape, the diffusion equation that must be solved for steady state interface shape, using coordinates moving with the tip is:

$$D\nabla^2 C + V\frac{\partial C}{\partial x} = 0 \quad \text{----------} (78)$$

where C = composition in atom fraction
V = velocity of interface in x-direction

The continuity of matter equation must be satisfied everywhere on the solid-liquid interface:

$$V_n (C_I^L - C_I^S) + D\frac{\partial C}{\partial \bar{n}} = 0 \quad \text{----------} (79)$$

where V_n = velocity normal to interface

I = interface, L,S liquid and solid respectively

$\frac{\partial C}{\partial n}$ = concentration gradient normal to interface

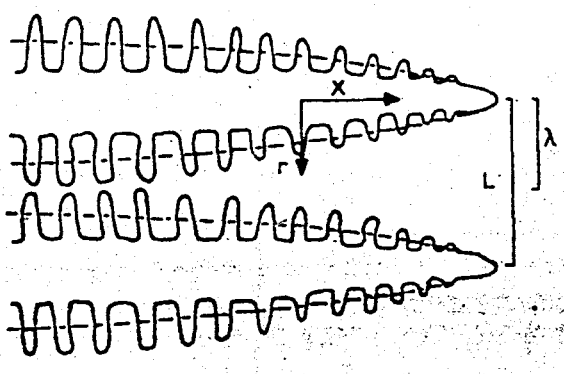

Fig.40[33]

Schematic dendrites: the dotted line shows the smooth shape assumed in Hunt's model; the figure also shows the definitions of x, r, λ and L.

Also an equation which relates temperature, composition and curvature must be satisfied in solid-liquid interface. Neglecting kinetic undercooling:

$$\Delta T = \Delta T_b + \Delta T_d \qquad (80)$$

where $\Delta T = T_o - T_I$

$\Delta T_b = m(C_o - C_I)$

$\Delta T_d = \theta(R_1^{-1} - R_2^{-1})$

T_o and C_o are temperature and composition of the starting alloy at equilibrium on a flat solid-liquid interface respectively, R_1 and R_2 principal radii of curvature, θ is curvature undercooling constant at constant liquid composition.

The volume element times the rate of change of composition must be equal to the difference in the material diffusing in and out of the element, plus that rejected into the element due to freezing. Considering Fig.41:

$$g_L \frac{\partial \bar{C}}{\partial t} = \frac{\partial [D g_L \partial \bar{C}/\partial x]}{\partial x} + \bar{C} C_k - \frac{D \partial g_L}{\partial t} \quad \text{-------(81)}$$

where g_L = fraction of liquid

$\bar{C}$ = average liquid composition, assumed to equal to C

t = time

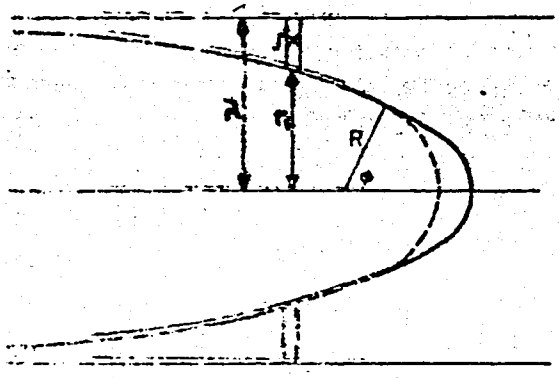

Fig.41[33]

Schematic view of hypothetical dendrite growing with homogenous liquid in the r direction but some diffusion in x direction

Assuming the temperature gradient in the liquid (G_L) is constant and integrating Eq.81 between the boundary conditions $\bar{C} = C_T$ at $g_L = 1$ and $\bar{C} = C_x$ at $g_L = g_L$;

$$g_L^{(k_o-1)} = \frac{C_1 (1-k_o) + (D G_L / m V)}{C_T (1-k_o) + (D G_L / m V)} \quad \text{----------(82)}$$

Relating g_L to r_1 and λ from Fig.41, an expression giving the hypothetical shape of dendrite is obtained, which grows with the liquid homogenous in r direction but with some diffusion in the x direction. Near the tip, the liquid is not homogeneous in the r direction, therefore an approximation is obtained by fitting a part of a sphere to the derived shape, as shown by dotted line in Fig.41. Since $r_1^2 / \lambda^2 \ll 1$, and the tip radius is $R = r_1 / \sin\phi$; letting $\phi = 45°$:

$$R = - G_L \lambda^2 / \sqrt{2} \left[m C_T (1-k_o) + D G_L / V \right] \quad \text{----------(83)}$$

Kurz and Fisher[34] applied the LM-K principle to alloy dendrites growing in a positive temperature gradient to develop a relationship between growth conditions and dendrite tip radius. Equating the dendrite tip radius to the wavelength of instability of the solid-liquid interface, curvature undercooling was neglected because growth was expected to occur at large radii of curvature. The shortest wavelength perturbation which will grow and lead to instability is estimated as:

$$\lambda_c = \lambda = 2\pi \left(\frac{\Gamma}{m G_c - G_L} \right)^{1/2} \qquad (84)$$

where Γ = Gibbs-Thomson parameter (γ_{LS}/S)

G_c = concentration gradient in the liquid at the interface

and defining G_c as

$$G_c = \frac{C_o}{R/2 - D/V_p} \qquad (85)$$

where $p = 1 - k_o$

Equating $\lambda = R$,

$$R = \frac{2D_L}{V_p} + \frac{2m C_o}{G_L} \quad \text{at low V} \qquad (86)$$

$$R = 2\pi \left(\frac{D\Gamma}{V k_o \Delta T_o} \right) \quad \text{at high V} \qquad (87)$$

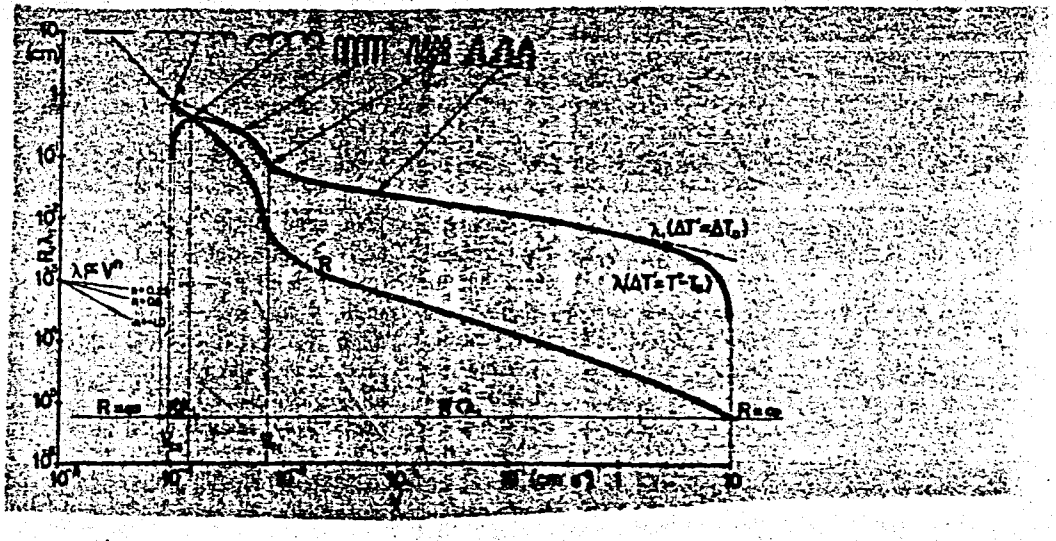

Fig.42[34]

Tip radius R and primary arm spacing λ_1 as a function of V. (Al-2wt%Cu, G_L=100Kcm^{-1}) The diagram indicates the interface morphology to be expected in different growth regimes.

In the first approaches to dendrite sidebranch evolution mechanism,[35] Temkin's optimized steady state solution was accepted as the pertinent growth condition at the tip of a branching dendrite. The thermal diffusion associated with the branch perturbation was assumed to be at steady state as in the growth of basis needle dendrite. According to this model (standing wave model), whole dendrite will grow at a steady state,i.e., the branched regions of dendrite as well as the dendrite tip will propagate at a constant velocity in the direction of the dendrite main axis preserving the undulatory shape. In this calculation, a perturbation source is believed to be necessary to initiate the branching instability.

More recently, Langer and Müller-Krumbhaar developed a time-dependent model. In the LM-K theory, since the marginal stability condition is used to select the steady state of the dendrite tip, the tip is the only point in needle dendrite which is stable. Instability persists at all the other portions of the dendrite surface and lead to sidebranch formation. Therefore, the evolution of the dendrite sidebranches is due to intrinsic morphological instability of the needle dendrite (except at the tip) which does not need to be induced by growth fluctuations at the dendrite tip. Later experiments performed by Huang and Glicksman agreed well with this conclusion.

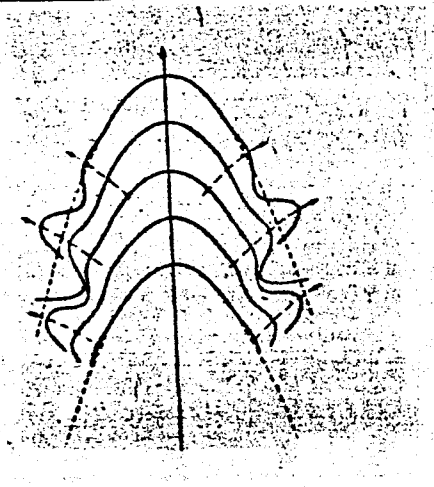

Fig.43
The LM-K model for dendrite sidebranching mechanism.

2.3.2 Dendrite Arm Spacing

A typical dendrite can be visualized in terms of the structure schematically portrayed in Fig.44, which has a primary structure and secondary and higher order arms or branches.

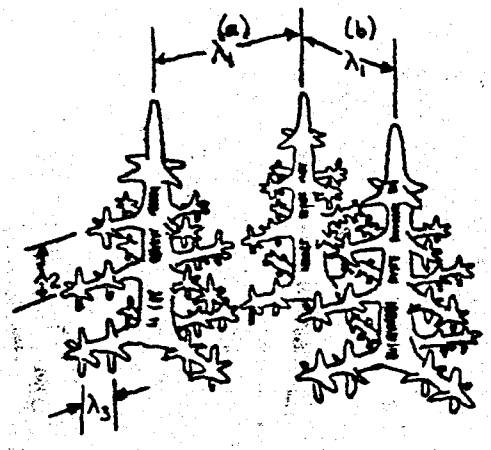

Fig.44
Primary, secondary and tertiary dendrite arm spacings

Generally dendrite arm spacings are measured as the perpendicular distances between the branches.

Studies on transparent alloys show that columnar dendrites can adjust their primary spacing during growth without difficulty. If spacing is too close, one or another primary arm falls behind and is subsequently engulfed. If spacing is too large, a tertiary arm growing from a secondary arm catches up to the growing primary tips and becomes one of them, as sketched in Fig.45

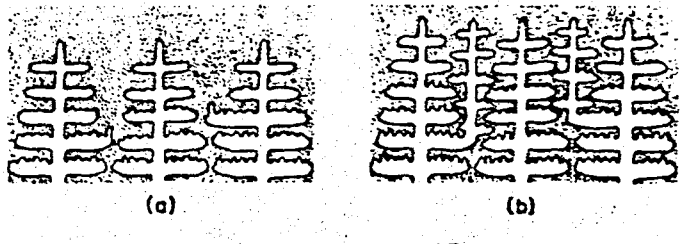

Fig.45 [36]
Forming of new dendrite arms by branching from secondaries

The driving force for this mechanism of spacing adjustment is constitutional supercooling in the region between the two primary dendrite arms. The dendrite is able to branch sufficiently to reduce this supercooling to a very low value.

It has been shown[37],[38] that the final secondary dendrite arm spacings that are measured in a fully solidified casting is usually more coarser than the one that forms initially. The coarsening comes about because some of the arms which form initially become unstable later in solidification and melt while others continue to grow. These are the dendrites which have radius of curvature which is smaller than average, therefore they grow more slowly than their neighbors or melt away. The constitutional supercooling which is sufficient near the dendrite tip to form the arms is reduced to such a low value back from the tips that the effect of the radius of curvature on melting point becomes relatively more important. The result is the remelting of some side arms.

2.3.2.1 Primary Dendrite Arm Spacing

The spacing between the primary dendrite arms has been found to depend upon factors such as: [34],[38],[39],[40],[41],[42]. Growth rate(R), Temperature gradient in the liquid at the liquid-solid interface(G_L) and solute content(C_o).

G.R.Kotler et.al.[39] formulated the spacing between the dendrite arms(λ_1) as:

$$\lambda_1^2 \propto \frac{1}{G_L R} \qquad \text{---------- (88)}$$

Rohatgi and Adams[Ref. 38] put the dendrite arm spacing as:

$$\lambda_1^2 = 8 D_L \Delta T / G_L R \qquad \text{---------- (89)}$$

where D_L = diffusion coefficient of solute in the liquid

ΔT = undercooling

$G_L = \frac{\Delta T}{\Delta x}$; and $R = \frac{\Delta x}{\Delta t}$

$\therefore$ G_R = cooling rate

Young and Kirkwood[38] worked with Al-Cu alloys and found a relation:

$$\lambda_1 = k G_L^{-a} R^{-b} \qquad \text{---------- (90)}$$

The data of [38] for a and b is given below:

w% Cu	a	b	K
2.4	0.50	0.50	5.65×10^{-3}
4.4	0.50	0.36	3.05×10^{-3}
10.1	0.50	0.43	4.65×10^{-3}

The results of Young and Kirkwood are plotted in Fig.46-48

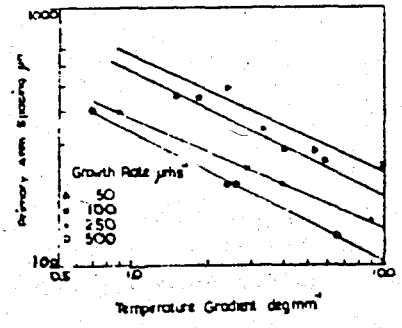

Fig.46 [38]
Primary dendrite arm spacing as a function of temperature gradients and different rates R for Al-4.4 w/O Cu

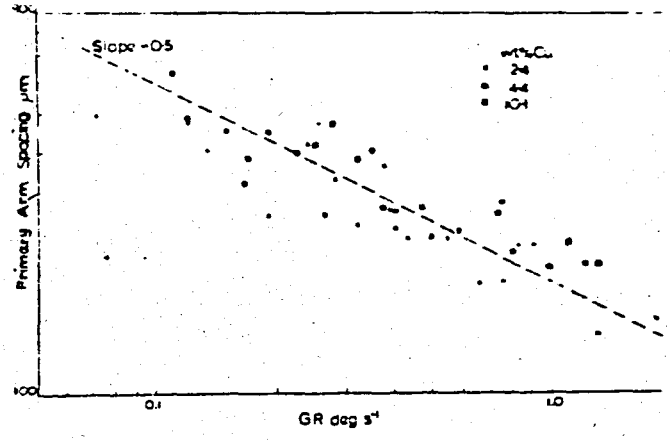

Fig.47 [38]
Primary dendrite arm spacing as a function of cooling rate $G_L R$

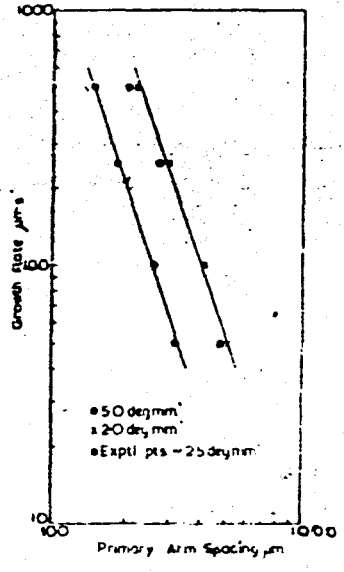

Fig.48 [38]
Primary arm spacing as a function of growth rate R, for Al-4.4 w/o Cu alloy

Klaren et.al.[43] and Jacobi and Schwerdtfeger[41] obtained similar results. (Fig.49-50)

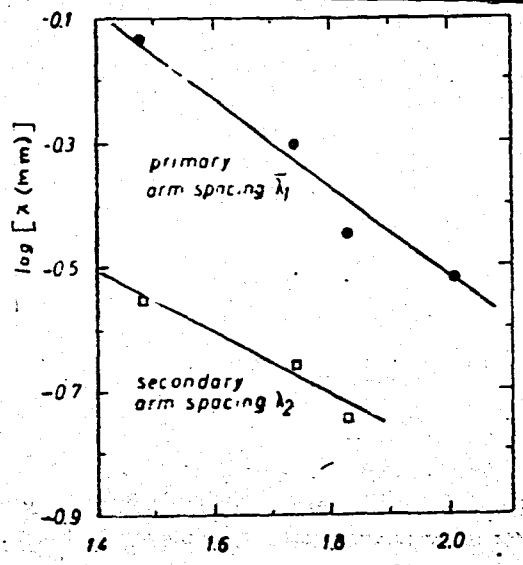

Fig.49 [41]

Influence of thermal gradient on primary and secondary spacing at a growth rate R=120 mm/hr for steel

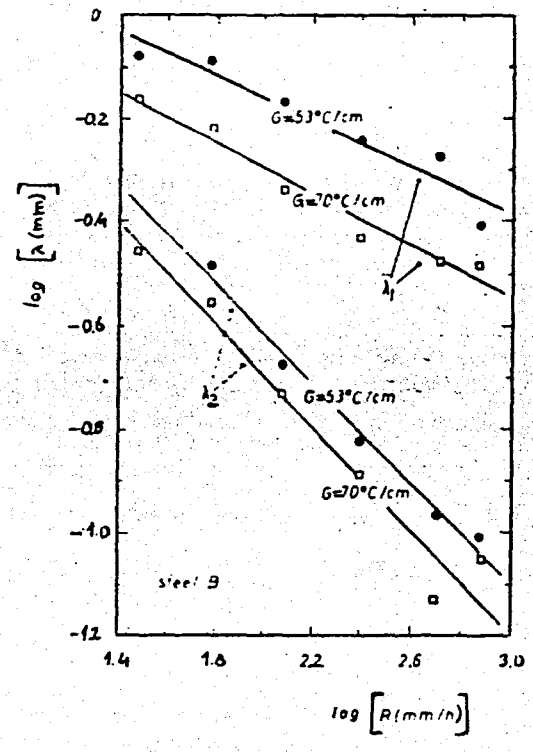

Fig.50 [41]

Influence of growth rate on arm spacings at constant thermal gradients for steel.

J.D.Hunt [33] found the primary dendrite arm spacing to be dependent as:

$$\lambda_1^4 = -64\,\theta\, D_L m (1-k_o) C_o / G_L^2 V \qquad (91)$$

$$\lambda_1 \propto G_L^{-1/2} \qquad (92)$$

$$\lambda_1 \propto V^{-1/4} \qquad (93)$$

where θ = curvature undercooling constant

Kurz and Fisher [34] stated that at high velocities

$$\lambda_1 = 4.3\,\Delta T'^{1/2} \left(D_L \Gamma / \Delta T_o k \right)^{1/4} V^{-1/4} G^{-1/2} \qquad (94)$$

and at low velocities

$$\lambda_1 = \left[\frac{G \Delta T'}{G_L P} \left(\frac{P\acute{e}}{V} \quad \frac{\Delta T_o k}{G_L} \right) \right]^{-1/2} \qquad (95)$$

where $\Delta T'$ = Difference between tip temperature and nonequilibrium solidus temperature

$\Delta T_o = T_L - T_s$ for C_o

$p = 1 - k_o$

Pé = Péclet number $VR/2D_L$

A table of results of various workers forming the λ_1 dependency as $\lambda_1 = kG_L^{-a}R^{-b}$ is given below. Table II.

Table II

Dendrite Matrix	Solute	b	a	Author
Pb	Sn 10-5 w.%	0.45	0.33	Klaren et.al
	Au 8	0.44	-	Klaren et.al
	Sb 2-7	0.42	-	Spittle
	Sb 5-10	-	0.35	Kotter
Al	Cu 2.2-10	0.43	0.44	Young
	5.7	0.36	-	Taha
Fe	Ni 8	0.19	-	Jin
	0.035 C, 0.3 Si	0.26	-	Alberny

The results observed by previous workers yield that primary arm spacing decreases with increasing temperature gradient or growth rate.

When the cooling rate is increased, the solidification takes place in a shorter time, therefore more dendrites have a chance to grow on. This leads to a decrease in dendrite arm spacing.

As the temperature gradient increases in front of the growing dendrite arms, the distance between the primary and secondary arms decreases. The reason for this is explained by Burden and Hunt[33] in this way: As the amount of undercooling decreases, the dendrite tip temperature increases. The amount of undercooling in this region is:

$$\Delta T = G_L D_L / R \qquad (96)$$

Accordingly, the distance between the dendrite arms will decrease.

There are different arguments about the effect of solutecontent with dendrite primary arm spacing.
In one of the first studies performed, Horward and Mondolfo[44] stated that dendrite arm spacing decreases with increasing solute content, without making a distinction between primary and secondary dendrite arm spacings.
Burden and Hunt[17] stated that undercooling increases with increasing solute content. Remembering

$$\lambda_1^2 = 8 D_L \Delta T / G_L R \qquad (97)$$

this implies that dendrite arm spacings will increase with increasing solute content.

Young and Kirkwood[38] stated that primary dendrite arm spacings increase but secondary dendrite arm spacings decrease with solute content.

Spittle and Lloyd[42] studied under a wide range of gradients with Pb-Sb alloys and observed that at high gradients the arm spacings are independent of composition and they increase with increasing solute content only at low gradients.

Results of Spittle and Llyod are seen in Fig.51 and 52.

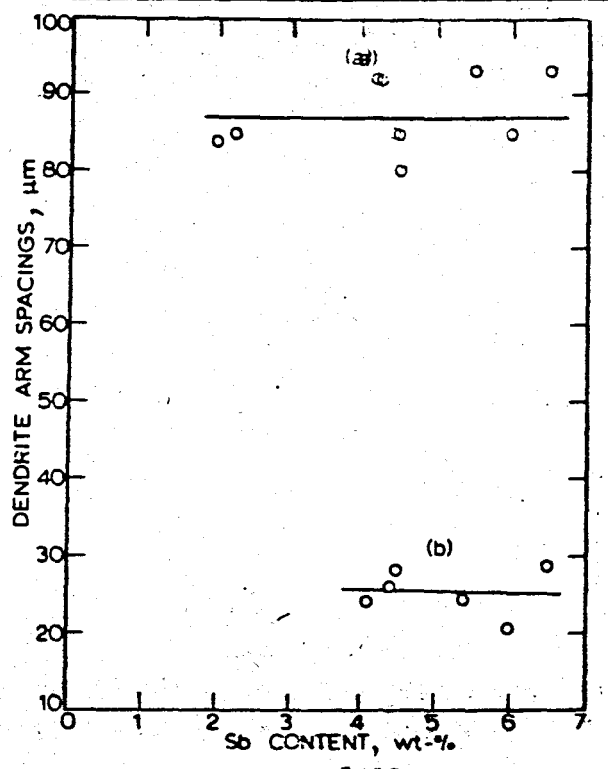

Fig.51[42]

a)primary arm spacing b)secondary arm spacing G_L= 2.3°C/mm
Change of dendrite arm spacings with solute content

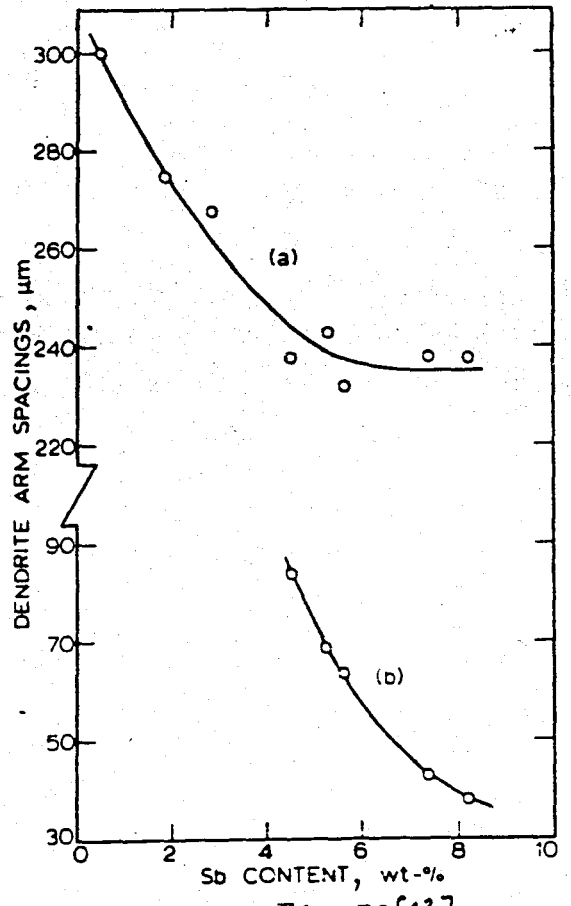

Fig.52[42]

Change of dendrite arm spacings with solute content G_L=19.7°C/mm

2.3.2.2 Secondary Dendrite Arm Spacings

The spacing between the dendrite secondary arms has been found to depend upon:[34],[38]-[43] Temperature gradient in the liquid at the solid-liquid interface(G_L), growth rate(R), solute content(C_o), the distance behind the dendrite tip(d) and local solidification time t_s which is defined as:

$$t_s = \Delta T_s / G_L R \qquad (98)$$

where $\Delta T_s = T_L - T_E$ nonequilibrium temperature range of freezing

$G_L R$ = cooling rate

Bower et al.[ref-38] related the secondary dendrite arm spacing as:

$$\lambda_2 = A d^n \qquad (99)$$

where d = distance behind the dendrite tip

A, n = constants

Spittle and Lloyd,[42] Jacobi and Schwerdtfeger,[41] Klaren et.al[43] put the relationship between spacing of dendrite arms as:

$$\lambda_2 = G_L^{-a} R^{-b} \qquad (100)$$

Table II applies to secondary dendrite arm spacings also.

As the velocity of primary dendrite tips increase(R), solute build up also increases at the tip. This leads to a lower gradient within the grooves of the secondary dendrite arms, and the grooves may widen with the consequence that coalescence is inhibited. Therefore secondary dendrite arms are expected to decrease with increasing growth rate.

Also, the increase of R is expected to lead to a larger decrease in λ_1 than λ_2 since secondary arms coalescence to give larger spacings while primary arms are geometrically incapable of altering their spacing.

3. Experimental Details

In the present work primary and secondary dendrite arm spacings in Al-2wt.%Cu alloys unidirectionally solidified under steady state conditions is investigated.

3.1 Experimental Programm

Previous studies on Al-Cu alloys [18], [33], [38] have agreed on the relationship:

$$\lambda_1 \propto G_L^{-a} R^{-b} \qquad (101)$$

where λ_1 represents the primary dendrite arm spacing, i.e. the distance between the stem of dendrites lying parallel to the heat flow, and a and b are constants. However, there seems to be a discrepancy about the values of the constants a and b. Young and Kirkwood [38] obtained $a = b = 0.5$ and put the relationship as:

$$\lambda_1 \propto (G_L R)^{-0.5} \qquad (102)$$

J.D.Hunt suggested a relationship in the form: [33]

$$\lambda_1 \propto G_L^{-0.5} R^{-0.25} \qquad (103)$$

and varified it using the results of Sharp and Hellawell [18]. The worker also suggested that the results of Young and Kirkwood may be fitted in the relation of Eq.103. The temperature gradients used in Young and Kirkwood study is 7.5-130°C/cm and the growth rates are $5\text{-}50\times10^{-3}$ cm/sec, yielding a cooling rate range between $3.75\text{-}650\times10^{-2}$°C/sec for Al-2.4wt.% alloy. It is notable that Young and Kirkwood values for growth rate do not go much below the critical growth rate estimated by Burden and Hunt [26] as about 7×10^{-3} (Fig.36). Burden and Hunt demonstrated that for a large range of temperature gradients, (0.5-60°C/cm) the tip temperature increases with increasing velocity, for growth rates lower than about 7×10^{-3} cm/sec. Though Young and Kirkwood conclude in their study that primary dendrite arm spacing is not expected to get increasingly large as cooling rate becomes very small, and predict a possible break in the λ vs. $G_L R$ graph, no experimental verification is given for this argument.

In Sharp and Hellawell study, high gradients of 48-164°C/cm and moderate growth rates between 4.7-16x10^{-3} cm/sec were used leading to a cooling rate range of .225-2.624°C/sec for Al-2wt.%Cu alloy. The cooling rates used in the work of Sharp and Hellawell correspond to higher gradients and lower cooling rates than those employed by Young and Kirkwood.

In this study, moderate temparature gradient ranges(10-40°C/cm) but a high growth rate range (1-50x10^{-3} cm/sec) is chosen to be able to check the discrepancy observed in the dendrite arm spacing vs. growth conditions data.

The lowest growth rates employed (1x10^{-3},2x10^{-3}) are well below the critical growth rate estimated by Burden and Hunt, and it is expected that the possible break in the graph should occur within this range.

No complete agreement has been reached about the change of secondary dendrite arm spacing with growth conditions. Various workers suggest that secondary dendrite arm spacings decrease with increasing growth rate and temperature gradient following relation set in Eq.101, with same a and b values as primary dendrite arm spacing.[41],[42],[43]. Other workers [38],[39] have observed different changing trends in primary and secondary dendrite arm spacings. Young and Kirkwood[38] claim that primary dendrite arms decrease more with increasing growth rate compared to secondary arms. Kotter et.al. [39] suggest that the effect of increased growth velocity is more on secondary dendrite arm spacings, whereas temperature gradient increases effect primary dendrite arm spacings much more than secondary dendrite arm spacings, which almost grow independent of temperature gradient.

The ranges of temperature gradient and growth rate used in this study will be sufficient to check this discrepancy.

3.2 Apparatus

The apparatus used for unidirectional solidification is shown in Fig.53 and 54. The system consists of a Nichrome resistance growth furnace, a temperature controller and a drive system.

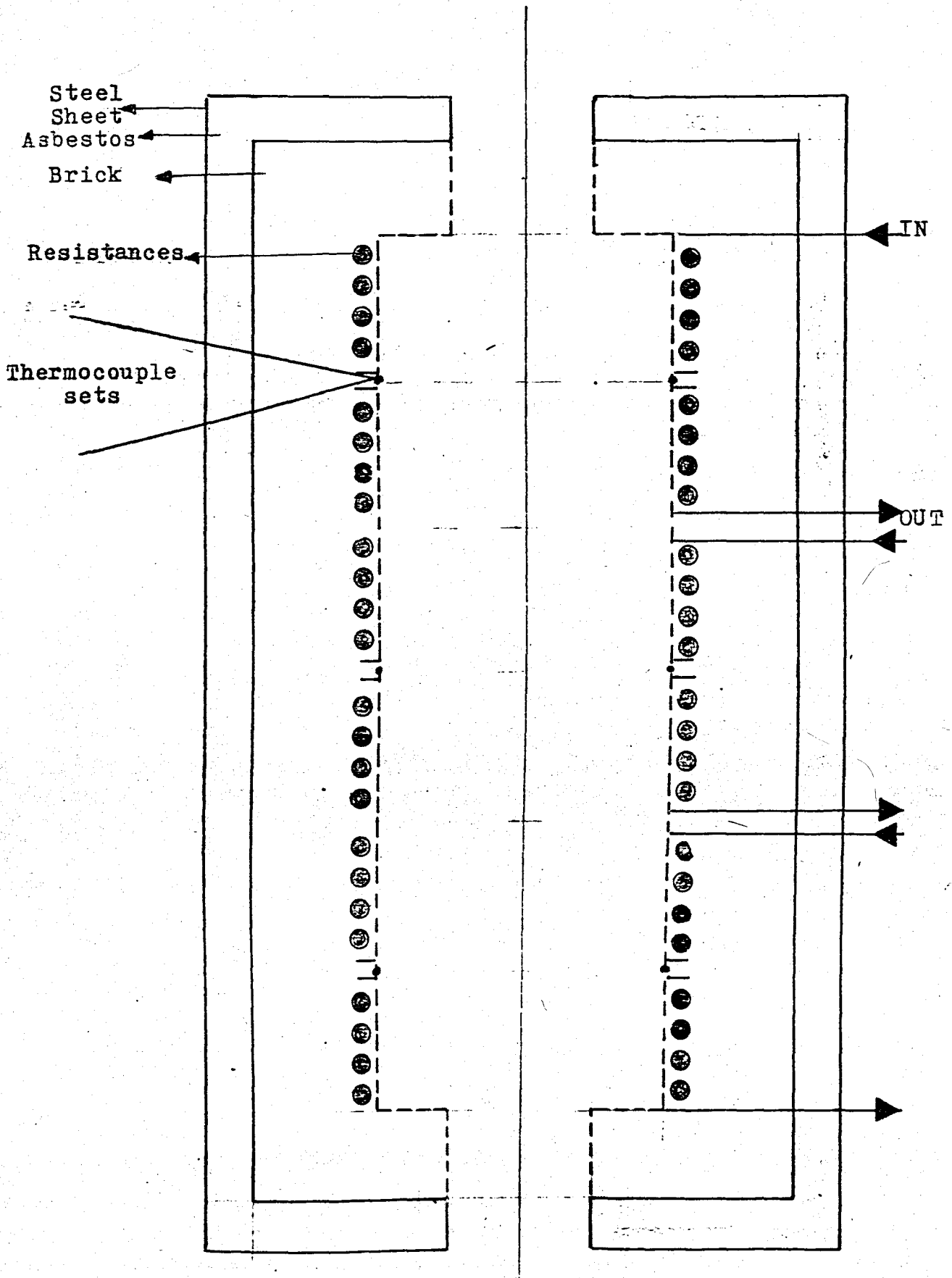

Fig. 23
Schematic view of the furnace

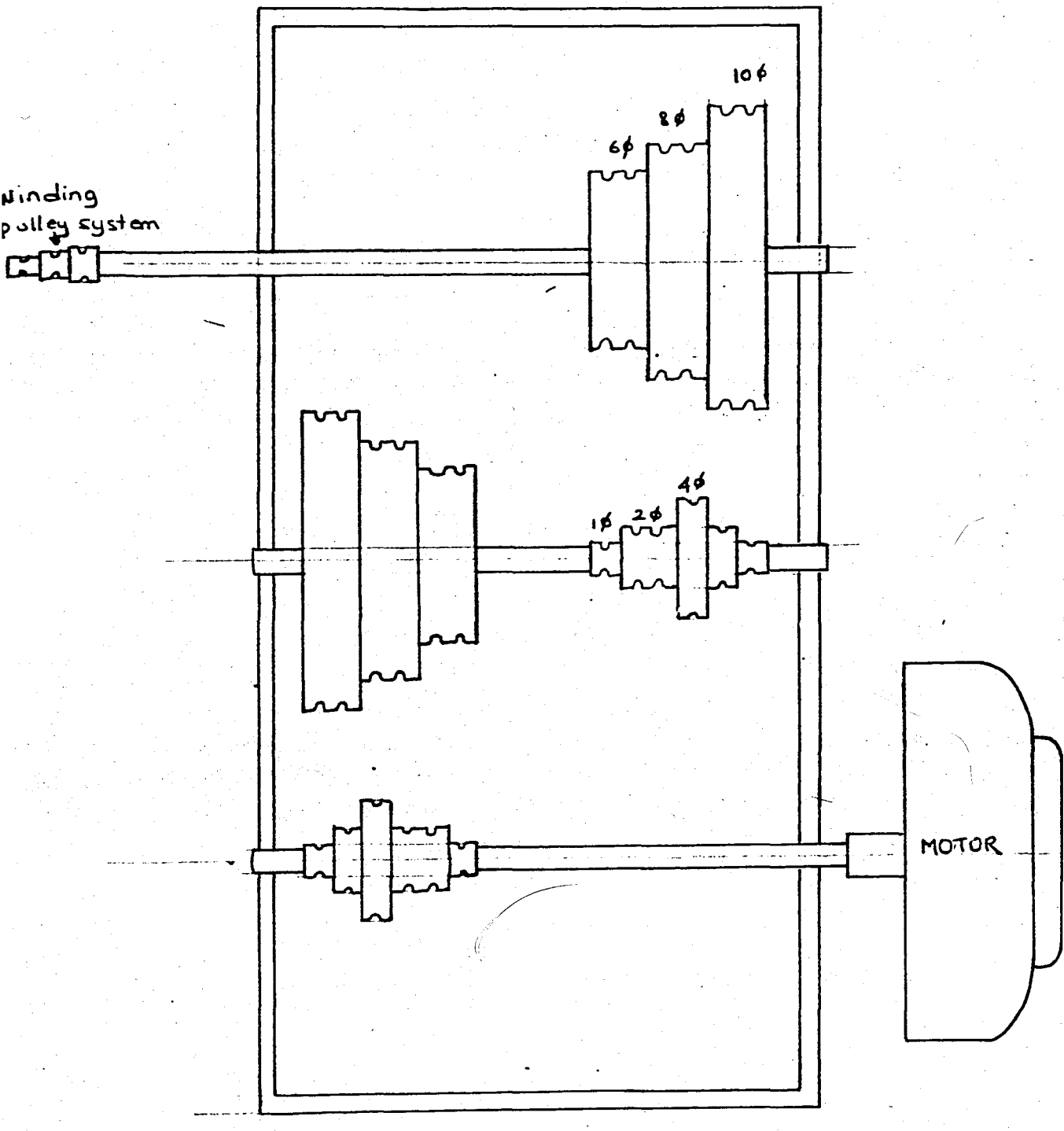

Fig 54
A schematic view of the drive set

3.2.1 Growth Furnace

The growth furnace is in 14X14X30 cm. dimensions and it contains three separate heaters,(Fig.53) each controlled by a set of chromel-alumel thermocouple inserted exactly in the middle of the heater. These thermocouple sets are connected to a thermostat(Elimko control unit) and set up the temperature gradient in the furnace. Another set of thermocouple is inserted from the other side of each heater which is connected to the potentiometer. This set checks the value displayed on the control unit so that a sound temperature gradient may be obtained.

Each heater has a power of 320 Watt. The inlets and outlets of windings are taken out through the insulating bricks and asbestos and connected to power supply.

3.2.2 Drive System

The drive system is used to lower the specimen into the furnace in the desired speed. It consists of a pulley system. 1-10 cm in diameter, and a winding pulley set $3/\pi, 4/\pi, 5/\pi$ cm. in diameter. By making different combinations in the pulley system and using a 2 rev/min motor, a large speed range from $1\text{-}148\times10^{-3}$ cm/sec may be obtained.(Fig.54)

3.2.3 Growth Rods

For unidirectional solidification experiments, growth rods are prepared by filling the alloy into a steel mold with two 100 mm. long, 4 mm ∅ holes as shown in Fig.55. Two growth rods at a time may be obtained with this mold.

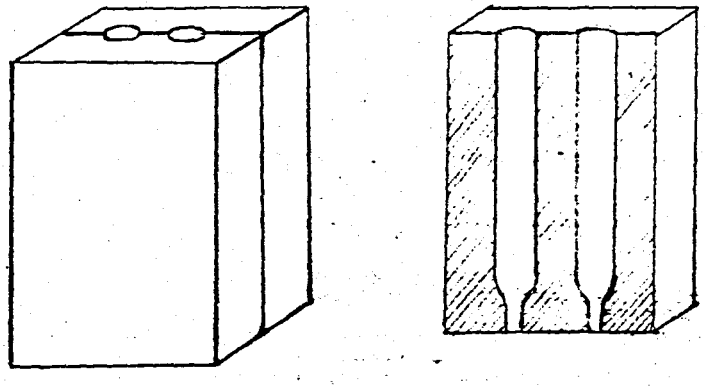

Fig55
Steel mold for growth rod preparation

4. Procedure

4.1 Alloy Preparation

In the preparation of Al-2wt.% alloy, superpure(99.999%) Al and cathodic copper(99.99%) is used. During the alloy preparation, first the necessary amount of aluminum is melted in a graphite crucible in a resistance furnace. Then the necessary amount of copper is added. The liquid metal is stirred with a graphite rod to homogenize the melt.

4.2 Unidirectional Growth

In unidirectional solidification process, a sound temperature gradient is very important. In this study, the temperature in each heater is arranged so that a linear temperature gradient is established. After setting the three temperature control units to predetermined temperature values, an hour is allowed for the temperature gradient to stabilize within the furnace. Data is taken every fifteen minutes from the second thermocouple set leading to the potentiometer to check the gradient.

When no fluctiation in potentiometer measurements is obtained the specimen may be inserted in the furnace. The growth rods are placed in graphite pots of 10 mm length and 4 mm internal diameter. A steel weight is hanged at one end of the graphite pot to prevent vibration. The other end of the rod is connected to the winding pulley with a wire. After the temperature gradient is rechecked, the motor is started and the growth rod moves down the furnace with predetermined speed.

After the predetermined period of growth, the wire is cut and the rod is let to fall down into the water tank placed at the bottom of the furnace to retain growth structure by quenching. Then the graphite rod is broken and sample is obtained.

4.3 Metallographic Examination

For metallographic examination, the quenched specimen is carefully cut from about ten mm behind the dendrite tips. This portion is used as the transverse section for primary arm spacing measurements. The longitudinal section is used for

secondary dendrite arm measurements.

The cut sample is mounted using optical mounting powder in the hot mounting apparatus. This is done to ease the polishing and microscopic examination of the sample.

The mounted sample is first rough polished to the middle of the rod. Then surface polishing is done using No.180,320,400 and 500 water polishing papers. A final surface polishing is done using abrasive cloths, and wetting with pure water mixed with metal oxides.

The polished sample is then etched using Kernel's reagent. (2 ml HF(48%),3 ml HCl(conc.),5 ml HNO_3 (conc) and 190 ml H_2O.) The sample is let to stay in this etchant for 8-15 seconds, washed and blown dry.

The revealed growth front may now be studied under microscope, and photographed. An Olympus microscope camera is used to take the photographs of the samples. (Magnification 60-120 times) The longitudinal section is photographed to reveal the secondary dendrite arms, and the transverse section is photographed for primary dendrite arm measurements.

Primary arm spacings are obtained by averaging 10 different measurements taken from the centers of the neighboring dendrites at the transverse section and averaging. Secondary arm spacings are obtained by averaging at least ten measurements taken from the longitudinal section at different distances behind the dendrite tip and averaging.

4. Results and Discussion

Results obtained for the unidirectional growth experiments of Al-2wt.%Cu alloy have been classified primarely with respect to the variation of primary and secondary arm spacings with temperature gradient(G_L) and growth rate(R); and cooling rate $G_L R$.

The measured variation of primary arm spacing(λ_1) with the experimental parameter G_L and R are tabulated in Table III

Table III

G_L °C/cm	R cm/sec	λ_1 mm
10	.001	.65
10	.002	.60
10	.0125	.45
10	.050	.27
20	.001	.62
20	.002	.50
20	.0125	.33
20	.050	.22
30	.001	.50
30	.002	.45
30	.0125	.30
30	.050	.135
40	.001	.50
40	.002	.43
40	.0125	.27
40	.050	.12

The graphical translation of the data reveals an important aspect of dendritic mdrphology in Al-2%Cu alloy.(Graphs 1, 2,3. in Appendix.)

In Graph 1 a plot of log λ_1 vs. log G_L has been drawn for each growth rate. This curve shows a high tendency to a straight line revealing an exponential relation between λ_1 and G_L. However, the graph indicates that log λ_1 vs. log

G_L curve is not parallel for differing growth rates as stated by some previous workers. The slopes of the lines vary between -0.21-0.6.

In Graph 2 log λ_1 vs. log R has been drawn for each temperature gradient. This curve also shows a high tendency for a straight line. However, again the lines for each graph are found to have differing slopes varying between -.22-.35 contradictory to the results of some previous workers[38] but in agreement with Jacobi and Schwerdtfeger.[41] On drawing only one line through all data points or averaging the slopes a slope of -0.28 is obtained.

Examination of the literature data on steady state growth reveals that the slopes of log λ_1 vs. log G_L and log λ_1 vs. log R curves are found to vary between approximately -(0.25-0.50) differing in value according to the working conditions and the alloy used. Almost all workers agree on the fact that λ_1 decreases with increasing G_L or R. Some of the previous workers have reported that changing the growth rate has no effect on the slope of log-log λ_1 vs. G_L lines. Kotler et.al.[39] have found the gradient exponent to be -0.35 and have also stated that the effect of R variation on λ_1 is greater than the effect of G_L. However no detailed explanation or varification on this statement takes place on their paper. Young and Kirkwood[38] have stated that the slopes of log λ_1 vs. log G_L and log λ_1 vs. log R have the same value approximately -0.5. These workers suggest in their paper that there is a possible break in the Al-Cu alloy dendrite arm spacing vs. growth conditions graphs, however no indication is given. The study of Taha[Ref.38] on Al dendrites in Al-Cu alloys at G_L:90°C/cm does not show a break in the log λ_1 vs. log R graph down to 8µm/sec and the rate exponent is found to be -0.36. In the Spittle and Lloyd[42] study the rate exponent is found to be -0.42 and a break in the log λ_1 vs. log R data was observed. Klaren et.al.[43] found the rate exponent as -0.44 and the temperature gradient exponent as -0.32. The theorethical work of Hunt[33] predicts that the

rate exponent is -0.25 and the temperature gradient exponent is -0.50.

In the present study no break in the log λ_1 vs. log R graph has been observed. However the slope of the decline seems to be less at lower R values(less than or equal to .002cm/sec). Since the slopes of log λ_1 vs. log G_L and log λ_1 vs. log R lines do not have the same value for differing R and G_L values, it is suspected that a combined effect of G_L and R, that is the cooling rate G_LR may be the correct parameter to be investigated. On Graph 3, λ_1 vs. G_LR relation is shown logarithmically. The dotted line represents the overall line when all data is considered. The slope of this line is found to be -0.29. The solid lines show a suspected break in the curve for high and low growth rates. The line correlation is higher when the data is divided as such and the relationship is in the form:

$\lambda_1 \propto (G_LR)^{-.21}$ for low growth rates

$\lambda_1 \propto (G_LR)^{-.47}$ for moderate and high growth rates

The slope found for higher growth rates agrees well with Young and Kirkwood data. However at lower rates a much smaller slope is obtained. In this range, the dendrite tip temperature increases with increasing growth rate(i.e. undercooling decreases) as predicted by Burden and Hunt.[26] The decrease in undercooling leads to a decrease in primary arm spacing. At the same time at low growth rates an increase in primary arm spacings is expected due to the lengthening of solidification time. However, the increase of tip temperature at this range decreasss the dendrite arm spacing and therefore the expected amount of increase is not observed.

The λ_1 vs. R and λ_1 vs. G_L graphs in this study reveal that the effect of these two parameters are not the same on primary arm spacings. When considered generally, it is observed that the slopes of primary arm spacing vs. growth rate lines are lower than those of temperature gradient.

However when each graph is carefully examined, it is seen that the temperature gradient is more effective on primary arm spacings at high growth rates. This effect gets lesser at low growth rates due to the above mentioned factor.

The log λ_1 vs. log R graph shows a lesser tendency to have higher slopes at higher temperature gradient values. Since the effect of temperature gradient on primary dendrite arm spacings is more ab obviously observed from the data, this change in slopes is explainable. The decrease in arm spacing due to the increase in growth rate will be more as the temperature gradient is also increased.

The measured variation of secondary dendrite arm spacing(λ_2) with experimental parameters G_L and R are tabulated in Table IV.

Table IV

G_L °C/cm	R cm/sec	λ_2 mm
10	.001	.14
10	.002	.10
10	.0125	.07
10	.050	.05
20	.001	.10
20	.002	.072
20	.0125	.05
20	.050	.035
30	.001	.07
30	.002	.052
30	.0125	.035
30	.050	.025
40	.001	-
40	.002	.043
40	.0125	.032
40	.050	.022

The graphical translation of data is in Graphs 4,5,6 and 7 in Appendix.

In Graph 4, the variation of secondary arm spacing with distance behind the growth front is logarithmically shown. Despite a slight scatter in measurements, the points confirm to a straight line with a slope of 0.32, yielding a relation in the form:

$$\lambda_2 \propto d^{0.32}$$

The reason of increase in secondary arm spacings is thought to be coalescence. Away from the tip the secondary arms thicken until their tips eventually touch and coalesce, leaving a solute rich film of liquid which shrinks and spheorodizes with further cooling. While taking data points, counting was abondened on each specimen at the observation of tip coalescence. The difference in data of workers using as-cast specimens may be due to this effect.

The log λ_2 vs. log R graphs for each G_L (Graph 5) yielded a straight line with slopes between -0.21-0.26. The extreme value of -0.21 is not very dependable since it was found with only three data points. Therefore it seems possible to average this relation as:

$$\lambda_2 \propto R^{-0.25}$$

The effect of growth rate on secondary dendrite arm spacings is not found to be more than on primary spacings as predicted by previous workers.

The log λ_2 vs. log G_L graphs drawn for each R value yielded straight lines with slopes between -0.59-0.61 which may be averaged as -0.60.

There has been disagreement between previous workers on the effect of temperature gradient and growth rate on secondary arm spacings. Young and Kirkwood[38] have stated that increasing the growth rate reduces the secondary arms due to the effect of increasing solute built up at the tips and increasing solute content behind the tips. This leads to a lower gradient within the grooves of liquid between the

secondary arms and the grooves widen with the consequence that coalescence is inhibited. Kotler et.al.[39] also agree on the fact that secondary arms decrease with increasing growth rate due to the decrease in the effective diffusion distance. However these workers expect a greater effect of R on secondary spacing than on primary spacings, and state that temperature gradient has no effect on secondary arm spacings. A more recent study by Spittle and Lloyd[42] reaches the conclusion that λ_2 decreases as G_L or R is increased. The data in this study is in agreement with the data in Jacobi and Schwerdtfeger[41] study in that the effect of temperature gradient on secondary dendrite arm spacings is more than the effect of growth rate. However before reaching such a conclusion with the present data, λ_2 vs. G_LR curve should be examined. It has been customary to relate the secondary dendrite arm spacings with G_LR or local solidification time t_s defined as:

$t_s : \Delta T_S/G_SR$ or
$t_s : \Delta T_S/G_LR$

where $\Delta T_s : T_L - T_E$

Since the alloy composition is constant in this study, it will be sufficient to regard the λ_2 vs. G_LR (cooling rate) curve.

As seen in graph 7, this curve gives a relation of

$\lambda_2 \propto (G_LR)^{-0.29}$

This result confirms with the results of Young and Kirkwood.[38]

Since a combined effect of temperature gradient and growth rate is acting on secondary dendrite arm spacings, the temperature gradient vs. secondary arm spacing results are not very reliable depending on the present data because a wider range of growth rates are used when compared to the range of temperature gradients and therefore when the data is seperated to find the effect of temperature gradient on secondary arm spacing, an exaggerated result(i.e. $\lambda_2 \propto G_L^{-0.6}$)

is reached. On the other hand, within the wide range of growth rates used, log λ_2 vs. log R graphs yield a more expected result.

6. Conclusion

It is concluded in this study that primary and secondary dendrite arm spacings in Al-2%Cu alloys decrease with increasing temperature gradient and growth rate. However the variation of λ_1 and λ_2 with growth conditions show different trends.

1) Primary arm spacing varies according to the relation

   $\lambda_1 \propto (G_L R)^{-0.21}$ for low growth rates

   $\lambda_1 \propto (G_L R)^{-0.47}$ for moderate and high growth rates

2) No such trend for a break is observed in the data of secondary dendrite arm spacing vs. growth conditions. However, the variation of λ_2 with cooling rate, expressed as

   $\lambda_2 \propto (G_L R)^{-0.29}$

   displays a lower tendency to change with growth conditions when compared to the primary arm spacings.

3) On the other hand, λ_2 has been found to vary with the distance behind the tip due to coalescence. This relation is formulated in the form:

   $\lambda_2 \propto d^{0.32}$

REFERENCES

(1) Chalmers,B.,"Principles of Solidification",John Wiley, New York 1967
(2) Weinberg,F. and Chalmers,B., Can.J.Phys.,1951,29,382
(3) Pfann,W.G.,, "Zone Melting", John Wiley, New York, 1966
(4) Tiller,W.A.,Jackson,K.A.,Rutter,J.W. and Chalmers,B. Acta Met., 1,428,1953
(5) Chalmers,B.,"Physical Metallurgy",John Wiley, New York, 1962
(6) Flemings,M.C.,"The Solidification of Castings and Ingots", John Wiley, New York, 1966
(7) Burton,J.A.,Primm,R.C.,Slichter,W.P., J.of Chem.Phys. V22, 11,1953
(8) Rutter,J.W.,Chalmers,B.,Can.J.Phys.,31,15,1953
(9) Hurle,D.T.J.,Solid State Electronics,1961,3,37
(10)Walton,D.,Tiller,W.A.,Rutter,J.W.,Winegard,W.C., Trans. AIME,203,1023,1955
(11)Glicksman,W.E.,Schaefer,R.J.,Ayers,J.D., Met.Trans. V76, 1976
(12)Morris,L.R.,Winegard,W.C., J.Crys.Growth, 6,361,1969
(13)Jackson,K.A.,Hunt,J.D.,Uhlmann,D.R.,SewardIII,T.P., Trans. AIME, 236,149,1966
(14)Bardsley,W.,Callan,J.M.Callan,Chedzey,H.A.,Hurle,D.T.J., Solid State Electronics, 142,3,1961
(15)Spittle,J.A.,Hunt,M.D.,Smith,R.W., J.Inst.Metals, 1964-65, 93,234
(16)Plaskett,J.S.,Winegard,W.C., J.Crys.Growth, 6,61,1969
(17)Tiller,W.A.,Rutter,J.W., Can.J.Phys., 34,96,1956
(18)Sharp,R.M.,Hellawell,A., J.Crys.Growth, 6,253.1970
(19)Cole,G.S.,Winegard,W.C., J.Inst.Metals, 92,322,1963
(20)Holmes,E.L.,Rutter,J.W.,Winegard,W.C., Can.J.Phys., 53, 1223,1957
(21)Coulthard,J.O.,Elliott,R. I.S.I. Publn. No 110, p.93, London, 1968
(22)Biloni,H.,Bolling,G.F.,and Cole,G.S., Trans AIME, 233,251, 1965

(23) Wineberg,F.,"Crystal Growth",Peiser,H.S.,Ed.Pergamon Press, 1967
(24) Kramer,J.J.,Bolling,G.F.,Tiller,W.A., Trans AIME, 227,374, 1963
(25) Backerud,L.,Chalmers,B., Trans AIME, 245,309,1969
(26) Burden,M.H.,Hunt,J.D., J.Crys.Growth, 22,99,1974
(27) Huang,S.C.,Glicksman,M.E., Acta Met., 29,701,1981
(28) Trivedi,R., J.Crys.Growth, 49,219,1980
(29) Nash,G.E.,Glicksman,M.E., Acta Met., 22,1283,1974
(30) Powell,G.L.F,Colligan,G.A.,Suprenant,V.A., and Urquhart,A., Met. Trans., V8A,971,1977
(31) Oldfield,W.,Mat.Sci.Eng., 11,211,1973
(32) Langer,J.S.,Müller-Krumbhaar,H.,Acta Met., 26,1681,1978
(33) Hunt,J.D.,"Cellular and Primary Dendrite Spacings",ISI Publishing,9,1977
(34) Kurz,W.,Fisher,D.J., Acta Met. V29,11,1981
(35) Tiller,W.A.,Kotler,G.R., J.Crys.Growth, 2,287,1968
(36) Flemings,M.C., "Modern Castings", 1964.46,353
(37) Allen,D.J.,Hunt,J.D., Met. Trans. 7A, May1976
(38) Young,K.P.,Kirkwood,D.H., Met Trans, V6A,197,1975
(39) Kotler,G.R.,Casey,K.W.,Cole,G.S., Met Trans. V3,723,1972
(40) Bell,J.A.E.,Winegard,W.C., J.Cryst.Metal, 92,357,1964
(41) Jacobi,H.,Schwerdtfeger,K. Met Trans, 7A,811,1976
(42) Spittle,J.A.,Lloyd,D.M., Paper in International Conf. of Solid.,p.15,Sheffield,1977
(43) Klaren,C.M.,Verhoven,J.D.,Trivedi,R., Met Trans, 11A, 1853,1980
(44) Horwarth,J.A.,Mondolfo,L.F., Acta Met V10,1037,1962
(45) Sharp,R.M.,Hellawell,A., J.Crys.Growth, 6,334,1970

APPENDIX

LIST OF GRAPHS

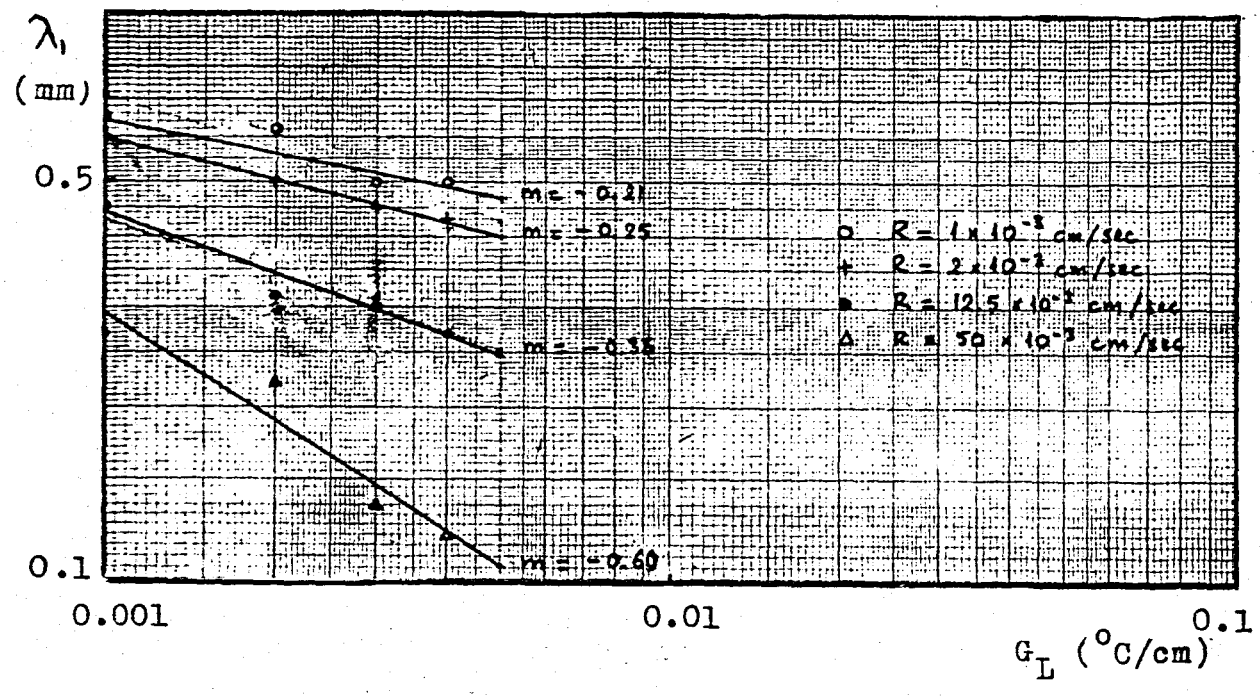

GRAPH 1. Primary dendrite arm spacing λ_1 vs. temperature gradient G_L.

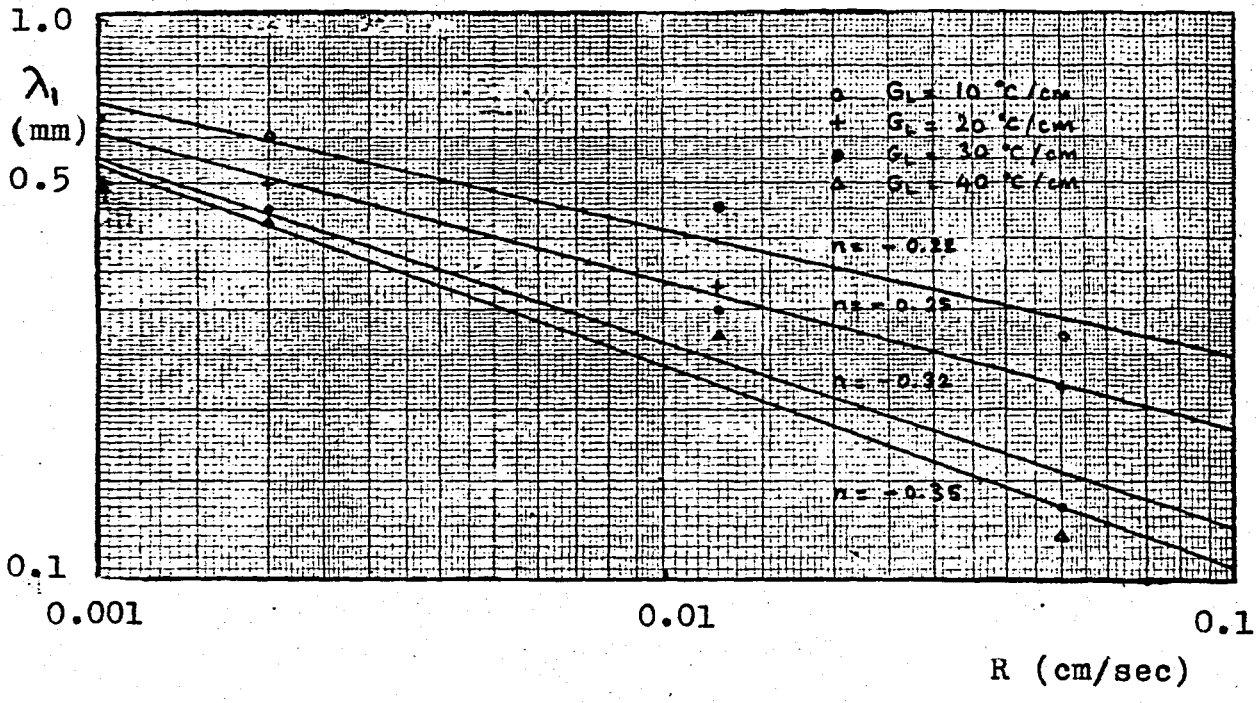

GRAPH 2. Primary dendrite arm spacing λ_1 vs. growth rate R.

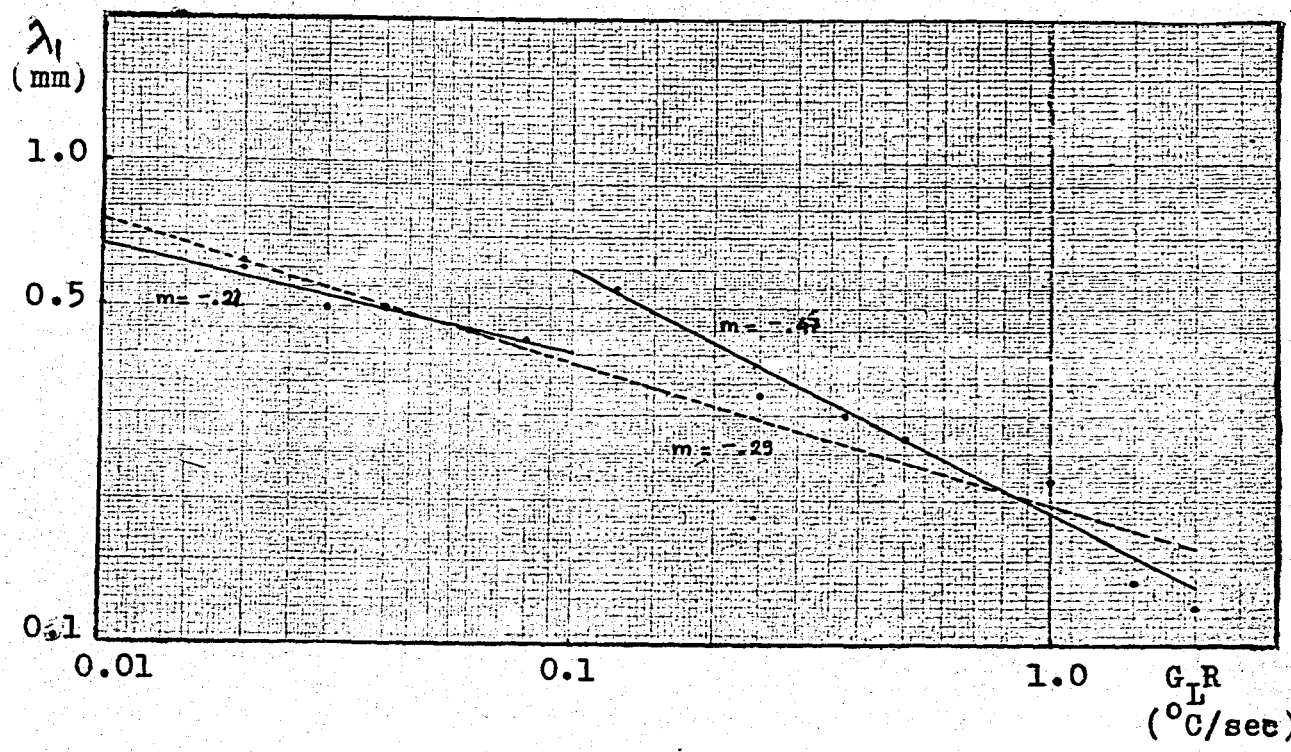

GRAPH 3. Primary dendrite arm spacing λ_1 vs. cooling rate $G_L R$.

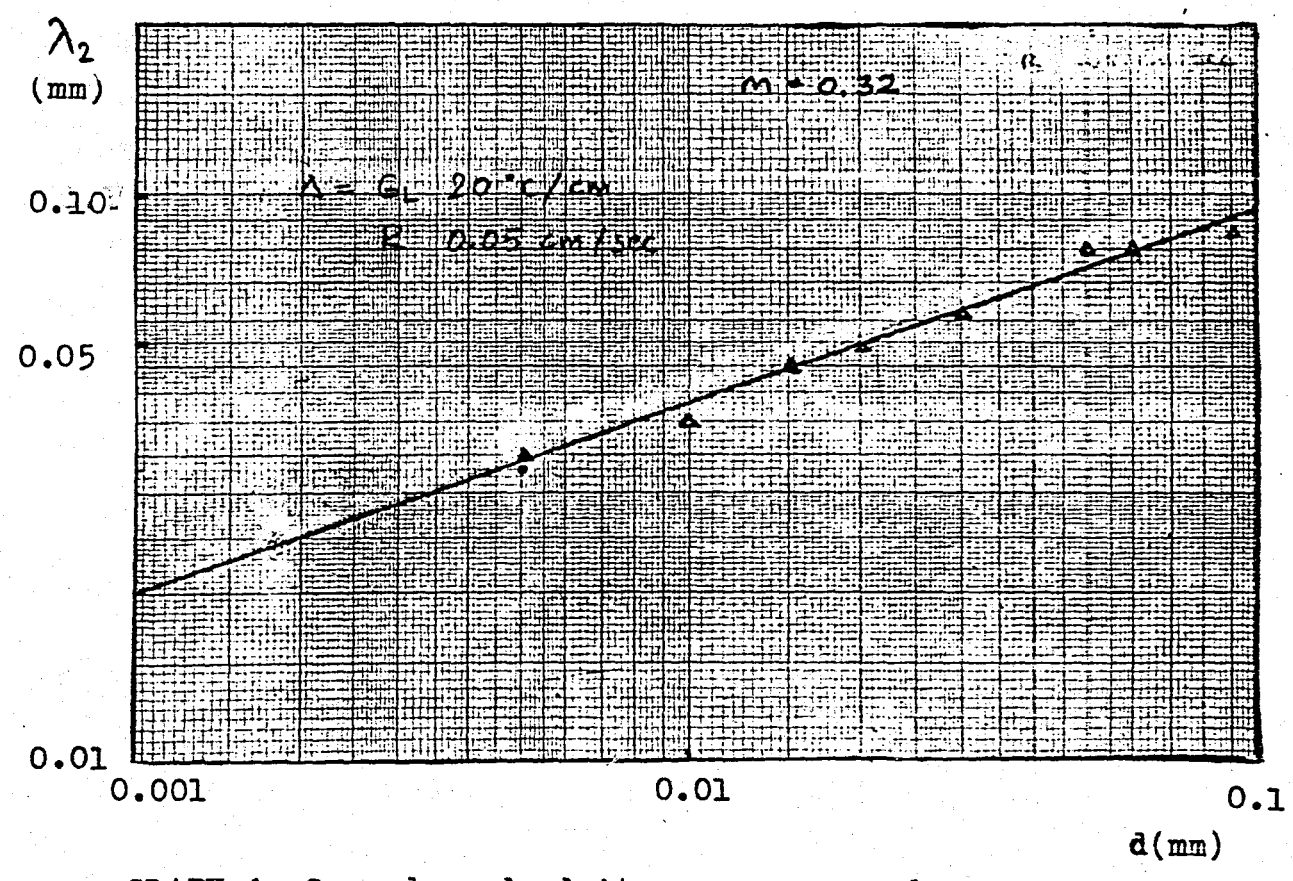

GRAPH 4. Secondary dendrite arm spaçing λ_2 vs. distance behind the dendrite tip d.

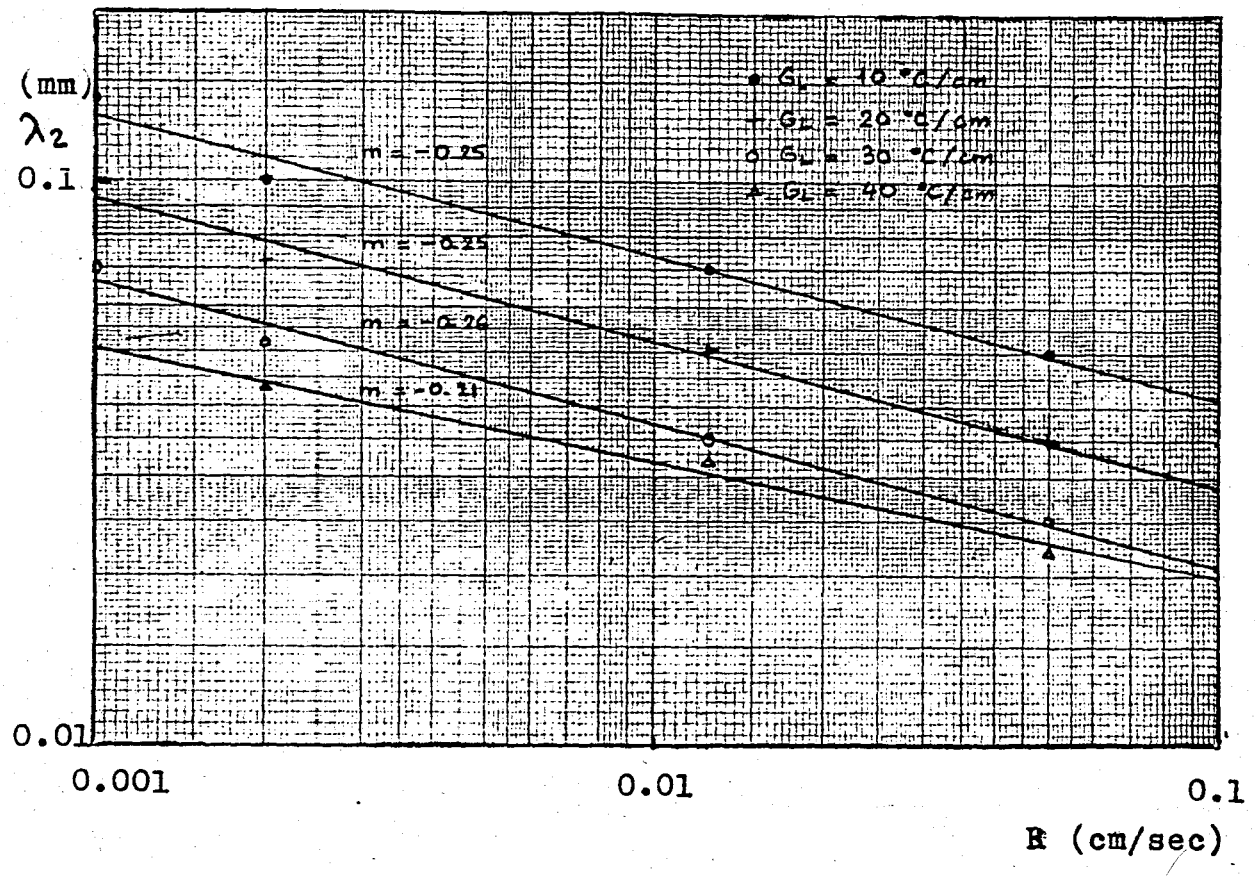

GRAPH 5. Secondary dendrite arm spacing λ_2 vs. growth rate

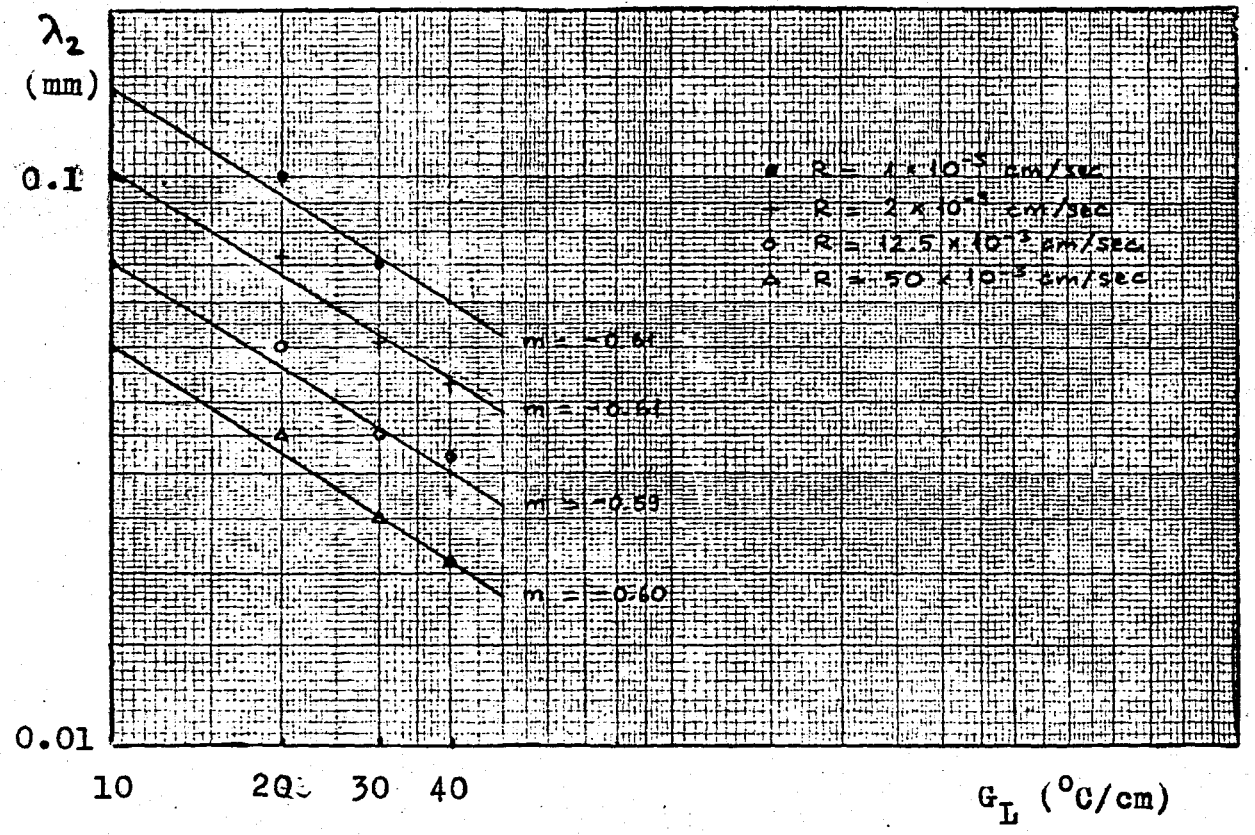

GRAPH 6. Secondary dendrite arm spacing λ_2 vs. temperature gradient G_L

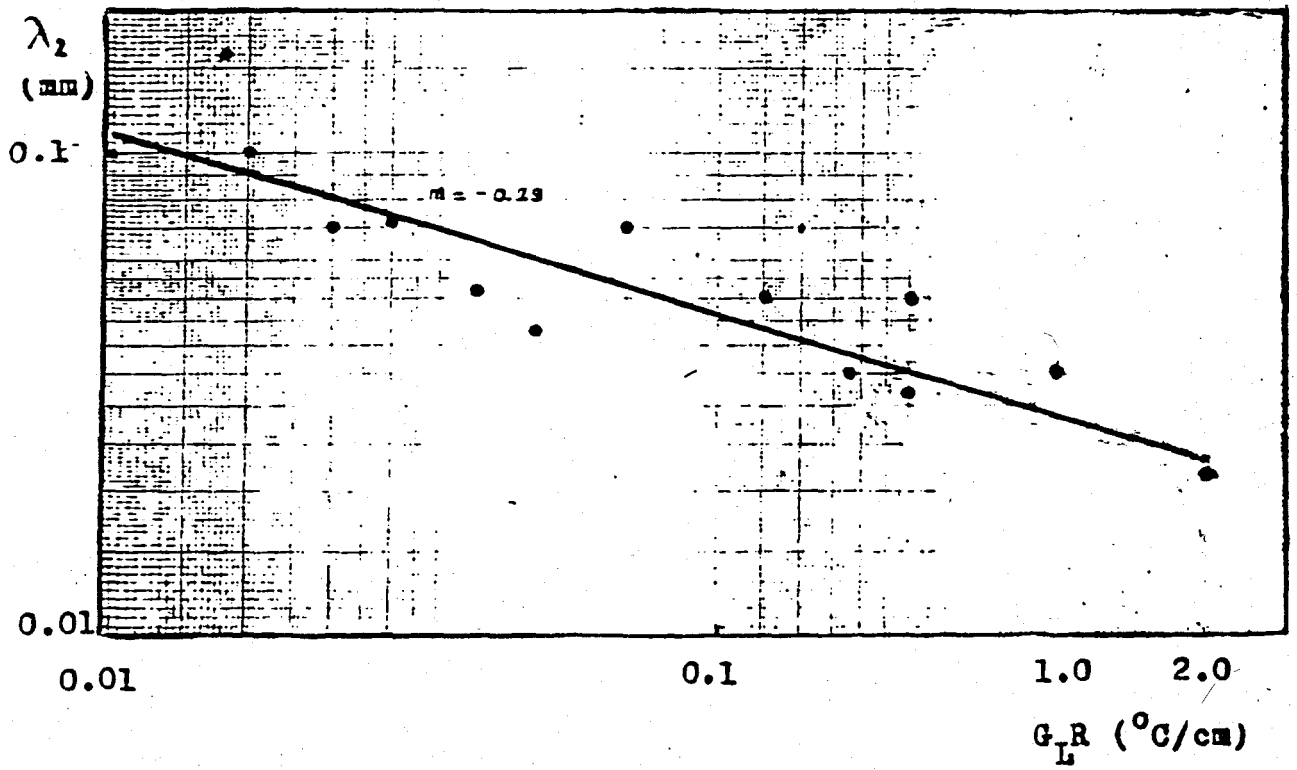

GRAPH 7. Secondary dendrite arm spacing λ_2 vs. cooling rate $G_L R$.